Journal of Geophysical Research: Earth Surface

RESEARCH ARTICLE
10.1029/2018JF004709

Response of Marine-Terminating Glaciers to Forcing: Time Scales, Sensitivities, Instabilities, and Stochastic Dynamics

Alexander A. Robel[1,2], **Gerard H. Roe**[3], **and Marianne Haseloff**[4,5]

[1]School of Earth and Atmospheric Sciences, Georgia Institute of Technology, Atlanta, GA, USA, [2]Division of Geological and Planetary Sciences, California Institute of Technology, Pasadena, CA, USA, [3]Department of Earth and Space Sciences, University of Washington, Seattle, WA, USA, [4]AOS Program, Princeton University, Princeton, NJ, USA, [5]Department of Earth Sciences, University of Oxford, Oxford, UK

Key Points:
- The marine-terminating glacier response to forcing occurs on two distinct time scales
- The glacier sensitivity to forcing depends on glacier state and nonlinearity in forcing processes
- The level of noise in nonlinear forcing processes can change the equilibrium state of a glacier

Supporting Information:
- Supporting Information S1

Correspondence to:
A. A. Robel,
robel@eas.gatech.edu

Citation:
Robel, A. A., Roe, G. H., & Haseloff, M. (2018). Response of marine-terminating glaciers to forcing: Time scales, sensitivities, instabilities, and stochastic dynamics. *Journal of Geophysical Research: Earth Surface*, *123*. https://doi.org/10.1029/2018JF004709

Received 9 APR 2018
Accepted 25 JUL 2018
Accepted article online 2 AUG 2018

Abstract Recent observations indicate that many marine-terminating glaciers in Greenland and Antarctica are currently retreating and thinning, potentially due to long-term trends in climate forcing. In this study, we describe a simple two-stage model that accurately emulates the response to external forcing of marine-terminating glaciers simulated in a spatially extended model. The simplicity of the model permits derivation of analytical expressions describing the marine-terminating glacier response to forcing. We find that there are two time scales that characterize the stable glacier response to external forcing, a fast time scale of decades to centuries, and a slow time scale of millennia. These two time scales become unstable at different thresholds of bed slope, indicating that there are distinct slow and fast forms of the marine ice sheet instability. We derive simple expressions for the approximate magnitude and transient evolution of the stable glacier response to external forcing, which depend on the equilibrium glacier state and the strength of nonlinearity in forcing processes. The slow response rate of marine-terminating glaciers indicates that current changes at some glaciers are set to continue and accelerate in coming centuries in response to past climate forcing and that the current extent of change at these glaciers is likely a small fraction of the future committed change caused by past climate forcing. Finally, we find that changing the amplitude of natural fluctuations in some nonlinear forcing processes, such as ice shelf calving, changes the equilibrium glacier state.

Plain Language Summary We develop a very simple mathematical model to explain how change in climate causes change in marine glaciers. The model shows that this response mostly occurs in two phases, a fast phase over tens to hundreds of years, and a slow phase over thousands of years. Glaciers have a larger response when they are on flat bedrock or when changes in the length of their ice shelf occur due to iceberg detachment. Even though some glaciers have not thinned or retreated significantly in recent years because they sit on steep downward sloping bedrock, they may experience rapid thinning and retreat in the future as they continue to respond to past climate change over thousands of years. Noise in climate and other processes that cause glaciers to be noisy can potentially cause permanent changes in glacier size. These results indicate that we should include noise when making predictions of glaciers changes so that we can calculate uncertainty in future projections and the impact of noise on permanent glacier size.

1. Introduction

Marine-terminating glaciers transport ice from the interior of ice sheets toward the ocean where ice melts or fractures into icebergs. Recent observations indicate that changes are underway in the speed, thickness, and terminus position of many marine-terminating glaciers in Greenland (Bjørk et al., 2012; Felikson et al., 2017; Moon et al., 2015) and Antarctica (Pritchard et al., 2009; Scheuchl et al., 2016). These changes are thought to be caused by long-term trends in climate, which drive surface melting (Fettweis, 2007; Mernild et al., 2011; Velicogna, 2009), ocean melting (Joughin et al., 2012; Rignot et al., 2010), and accelerated iceberg calving (Joughin et al., 2008; Nick et al., 2010).

It has long been understood that glaciers act as integrators of external forcing (Nye, 1960, 1963a, 1963b, 1965). Stochastic noise in climate forcing is integrated by glaciers on a characteristic time scale set by glacier

mass balance and geometry (Harrison et al., 2003; Jóhannesson et al., 1989), causing fluctuations of glacier thickness, flux, and length that are superimposed on the background glacier state (Lüthi, 2009; Oerlemans, 2000; Roe & Baker, 2014). Glaciers also respond to persistent changes in climate forcing on this characteristic time scale. Consequently, to evaluate whether recent retreat at individual mountain glaciers is caused by climate change or interannual variability, studies have compared the amplitude of stationary glacier variability (i.e., variability drawn from a distribution whose properties do not change in time) to the magnitude of nonstationary glacier changes caused by persistent trends in climate (Marzeion et al., 2014; Oerlemans, 2000; Roe & O'Neal, 2009; Roe et al., 2017). However, such comparisons are inherently difficult where records of glacier change are short compared to the slow response of glaciers to climate change.

In practice, complex numerical ice sheet models are used to calculate the discharge of ice from glaciers and predict the long-term response of marine-terminating glaciers to future climate change (e.g., Favier et al., 2014; Pattyn et al., 2012; Seroussi et al., 2017). However, recent studies have provided simple analytical expressions for the dependence of ice discharge on local topographic and glaciological conditions, derived from asymptotic analysis of glacier flow at the grounding line (Haseloff & Sergienko, 2018; Hindmarsh, 2012; Pegler, 2016; Schoof, 2007a; Schoof et al., 2017; V. C. Tsai et al., 2015). The balance between ice input from snowfall and ice discharge to the ocean sets the equilibrium glacier state and determines the stability of marine ice sheet grounding lines (Schoof, 2012). Consequently, these simple approximations for ice discharge are potentially useful tools for simulating marine-terminating glacier change without using a complex ice sheet model.

Simulations of nonstationary change in marine-terminating glaciers often neglect the stationary, high-frequency variability in climate forcing. However, Mantelli et al. (2016) showed that in marine-terminating glaciers with internally generated variability, the inclusion of realistic noise in accumulation and surface temperature forcing may cause variability at decadal to centennial time scales that do not arise in the absence of noise. Mulder et al. (2018) showed that noisy forcing can cause grounding lines to transition across reverse-sloping beds, with the likelihood of unstable retreat found to be greater than the likelihood of unstable advance. Such studies raise the possibility that together, noisy forcing and the internal dynamics of glacier flow produce glacier variability that should be considered when interpreting and simulating glacier change due to climate forcing.

In this study, we show that a simple model of ice fluxes in a marine-terminating glacier can accurately emulate the most significant components of stochastic and nonstationary variability that appear in a flowline model (section 2). We show (section 3) that stable marine-terminating glaciers respond to forcing on two characteristic time scales separated by 1 to 2 orders of magnitude. These time scales vary with equilibrium glacier state (which is set by internal dynamics) and become unstable at different thresholds of bed slope. We derive (section 4) the glacier sensitivities to step, trend, and stochastic fluctuations in external forcing. These expressions for the glacier sensitivity provide a first-order approximation of the glacier response to forcing without the need for a complex numerical model. We show that these sensitivities depend on equilibrium glacier state and the strength of nonlinearity in forcing processes. Finally, we show (section 5) that under certain circumstances, equilibrium glacier state depends on the strength of noisy forcing, indicating that marine-terminating glaciers are nonlinear, state-dependent integrators of external forcing. We conclude (section 6) with a discussion of the relevance of the time scales and sensitivities of the two-stage model, to observed variability of marine-terminating glaciers in Greenland and Antarctica. We also suggest approaches for simulating future marine-terminating glacier behavior that considers the role of noise in climate forcing and ice sheet processes.

2. Two-Stage Marine-Terminating Glacier Model

High-order numerical models are typically used to simulate the response of marine-terminating glaciers to external forcing (e.g., Favier et al., 2014; Pattyn et al., 2012; Seroussi et al., 2017). In this section, we show that a simple, two-stage model of a marine-terminating glacier (i.e., two stages of adjustment) can accurately emulate the forced variability simulated in a more complex model. This two-stage model clearly shows the role of different physical processes in the glacier response to forcing and is also simple enough to permit derivation of the characteristic time scales (section 3) and sensitivities to different types of forcing (section 4). We begin with the derivation of the two-stage model.

2.1. Model Derivation and Assumptions

The organizing principle of our two-stage model is tracking how ice enters, moves through, and then exits a marine-terminating glacier. We consider a marine-terminating glacier with length L and spatially averaged thickness H (schematic in Figure 1b). The length L spans the entire glacier domain from the ice divide (where

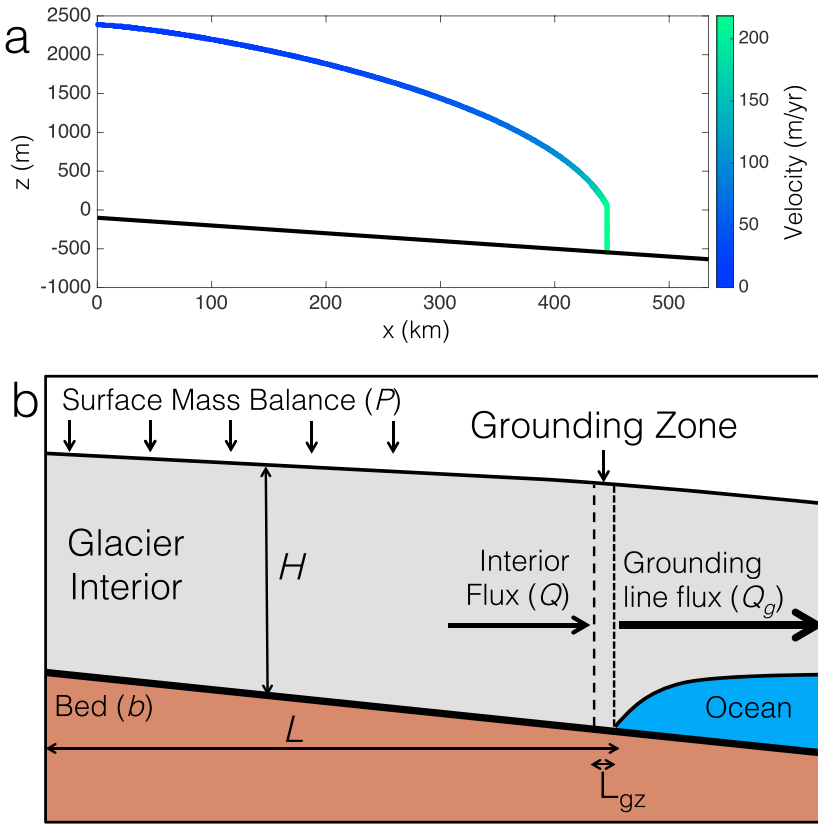

Figure 1. (a) Example of an ice thickness and velocity profile simulated by a flowline model of a marine-terminating glacier. See section 2.2 for model description. (b) Schematic of two-stage model. The bed geometry shown in schematic is purely illustrative.

there is no horizontal ice flow) to the grounding line. Consequently, we can take the total glacier ice volume to be $V = HLW$ where W is spatially averaged glacier width. The only way ice enters the glacier is through accumulation due to spatially averaged surface mass balance, P (the sum of accumulation and melting on the glacier surface). Ice leaves the glacier through a grounding line flux (Q_g),

$$\frac{dV}{dt} = W\left(PL - Q_g\right). \tag{1}$$

Carrying through the derivative, we rearrange to arrive at an equation for the evolution of spatially averaged glacier thickness

$$\frac{dH}{dt} = P - \frac{Q_g}{L} - \frac{H}{L}\frac{dL}{dt}. \tag{2}$$

where physically, the terms on the right-hand side are as follows: ice input due to spatially averaged surface mass balance, ice output due to divergence of ice flux through the grounding line ($\frac{Q_g}{L}$), and stretching due to changes in overall glacier length ($\frac{H}{L}\frac{dL}{dt}$).

In this study, we only consider scenarios where the time-averaged and spatially averaged surface mass balance ($\bar{P}$) is greater than zero, leading to a finite glacier length at steady state. We note however, that this does not exclude the possibility that the glacier can lose ice ($P < 0$) during transient time periods when surface melting exceeds accumulation through snowfall. We also note that climatological feedbacks may cause the surface mass balance to be dependent on variations in glacier geometry (as in Harrison et al., 2003), though we do not include such effects here under the assumption that they are small compared to ice flux feedbacks. If the width of the glacier in the grounding zone is different from the average width of the upstream catchment area of the glacier, we could also include a geometric multiplier on the surface mass balance term (i.e., PW_{UP}/W_{GZ}), which accounts for the fact that wide catchment areas may be funneled into narrow glacier outlets near the grounding zone. We do not consider such geometric complications in the idealized analyses in this study,

since the primary effect is to multiply the surface mass balance term. However, in using this simple model to approximate specific glaciers, such geometric considerations may be important.

The grounding zone is the region upstream of the grounding line (Figure 1b), with length L_{gz}, thickness h_g, and volume $V_{gz} = h_g L_{gz} W$. The grounding line is, by definition, the location where ice is sufficiently thin to float in seawater. Thus, the grounding line ice thickness is exactly at hydrostatic equilibrium with the local water depth,

$$h_g = -\lambda b(L), \tag{3}$$

where $\lambda = \rho_w/\rho_i$ is the ratio between the densities of seawater and glacial ice, and $b(L)$ is the depth of the bed below sea level at the grounding line. Thus, our model implicitly assumes that the glacier always remains marine-terminating. In order to consider a glacier terminus that is not at flotation, we would need to substitute this condition with another dynamical equation for terminus ice thickness and calving rate (as in Amundson, 2016). The length of the grounding zone is typically a few kilometers (for flat ice streams it may be tens of kilometers), which is much shorter than the length of the entire glacier ($L_{gz} \ll L$). Considering a local conservation of ice mass in the grounding zone, we assume that ice is advected into the grounding zone from the interior (Q) and is discharged by flux through the grounding line (Q_g),

$$\frac{\mathrm{d}V_{gz}}{\mathrm{d}t} = W(Q - Q_g), \tag{4}$$

where the additional flux from local surface mass balance (PL_{gz}) is assumed to be negligible. Carrying through the derivative on the left-hand side, as we did for the large-scale glacier evolution equation (equation (2)), we have

$$h_g \frac{\mathrm{d}L_{gz}}{\mathrm{d}t} + L_{gz} \frac{\mathrm{d}h_g}{dt} = Q - Q_g. \tag{5}$$

Since the grounding zone length is included within the full ice stream length ($L = L_{int} + L_{gz}$ where L_{int} is a quantity that we assume changes negligibly compared to the grounding zone, where most longitudinal stretching occurs in marine-terminating glacier), stretching and shrinking of the grounding zone length results in an equal change in glacier length (i.e., $\mathrm{d}L/\mathrm{d}t = \mathrm{d}L_{gz}/\mathrm{d}t$). We can then rewrite equation (5) as

$$\left(h_g - \lambda b_x L_{gz}\right) \frac{\mathrm{d}L}{\mathrm{d}t} = Q - Q_g, \tag{6}$$

where b_x is the local bed slope. Since b_x typically has the scale h_g/L (as assumed in Schoof, 2007a), we can generally say that $\lambda b_x L_{gz} \ll h_g$. Consequently, we can write the evolution equation for grounding line position as

$$\frac{\mathrm{d}L}{\mathrm{d}t} = \frac{1}{h_g}\left(Q - Q_g\right). \tag{7}$$

Since the grounding zone is very short, the grounding line flux in equation (7) has the form of a moving flux boundary condition that sets the grounding line position. Changes in grounding line position are directly caused by changes in the grounding zone flux balance ($Q - Q_g$), which may be influenced by far-field changes, such as fluctuations in upstream surface mass balance.

Equation (7) is combined with equation (2) to produce an evolution equation for the spatially averaged glacier thickness (H)

$$\frac{\mathrm{d}H}{\mathrm{d}t} = P - \frac{Q_g}{L} - \frac{H}{h_g L}\left(Q - Q_g\right) \tag{8}$$

Equations (7) and (8) form a complete two-stage dynamical model for the temporal evolution of a marine-terminating glacier. In this two-stage marine-terminating glacier model, ice enters through a prescribed surface mass balance, flows through the ice sheet interior toward the grounding zone, and then leaves as a grounding line flux. The first equation tracks the bulk mass flows through the marine-terminating glacier and the corresponding evolution of the glacier thickness. The second equation tracks the moving boundary condition at the downstream edge of the glacier that controls the magnitude of ice flux out of the glacier. The primary difference then, between this marine-terminating glacier model and previous simple models of mountain glaciers (e.g., Harrison et al., 2003; Jóhannesson et al., 1989; Lüthi, 2009; Oerlemans, 2000; Roe & Baker, 2014), is that mass loss occurs primarily through ice flux, rather than through negative surface mass

balance. If these two equations have a stable solution, they must be associated with, at most, two distinct time scales of glacier evolution (as we will see in section 3).

In marine-terminating outlet glaciers, ice in the glacier interior flows due to a combination of sliding at the base and deformation in the ice column. In this study, we will assume a very general form for interior ice flux

$$Q = \nu \frac{H^{\alpha}}{L^{\gamma}}. \tag{9}$$

This form generally holds when ice flux is occurring through a balance between gravitational driving stress ($\rho_i g H \frac{\partial H}{\partial x}$) and some resistive or shearing stresses within the ice or at the ice bed interface. For example, when there is a leading order balance between gravitational driving stress (where $\frac{\partial H}{\partial x} \approx \frac{H}{L}$) and basal shear stress set by a Weertman-style friction law (e.g., $Cu^{\frac{1}{n}}$ Weertman, 1957), the vertically -averaged ice flux is

$$Q = \left(\frac{\rho_i g}{C}\right)^n \frac{H^{2n+1}}{L^n}, \tag{10}$$

which gives $\alpha = 7$, $\gamma = 3$, and $\nu = \left(\frac{\rho_i g}{C}\right)^n$ for the commonly assumed value of the Glen's flow law exponent, $n = 3$. However, if we instead wanted to capture interior ice flux though vertical shear deformation within the ice column, then we would pick $\alpha = 8$ and $\gamma = 3$ (Cuffey & Paterson, 2010). By picking such a general form of the interior ice flux, we admit a wide array of possible choices for the processes driving interior ice flow. In this study, we use $\alpha = 7$ and $\gamma = 3$ to aid comparison between our simple model and more complicated models of marine-terminating glacier flow, many of which assume that ice flows through sliding in the glacier interior (e.g., Schoof, 2007a). In both cases, the H and L represent either global or spatially averaged quantities. The resulting flux from the interior (Q) represents the scale of interior ice flux that is purely a function of the large-scale glacier geometry. The advection of ice from upstream occurs through a spatially averaged flux, which does not resolve localized anomalies of ice geometry that may result in localized anomalies of ice flux. In section 6, we further discuss the consequences of such a spatially averaged ice flux.

Ice exits the grounded glacier by discharge through the grounding line or terminus. Various approximations for the ice flux through the grounding line have been developed, with different assumptions regarding basal friction and controls on ice shelf buttressing. However, regardless of particular assumptions, it is generally the case that the flux of ice through the grounding line or terminus (Q_g) is a function of the local ice thickness (h_g)

$$Q_g = \Omega h_g^{\beta}, \tag{11}$$

where β is an exponent that can be derived from asymptotic boundary layer analysis of the grounding line (Haseloff & Sergienko, 2018; Schoof, 2007a; Schoof et al., 2017; V. C. Tsai et al., 2015), other mathematical approaches (Hindmarsh, 2012; Lingle, 1984) or estimated empirically for tidewater glacier termini (Pelto & Warren, 1991). The Ω is a scalar parameter which incorporates the various factors (besides ice thickness) that can influence ice flux in the grounding zone or near the terminus. In this study, we primarily (except in section 2.2) use two versions of the grounding line flux derived in Haseloff and Sergienko (2018), which both assume strong buttressing by an ice shelf. In the limit that the ice shelf primarily loses mass through calving

$$\Omega = (n/2)^n (n+1)^{-(n+1)} \left[\rho_i g \left(1 - \lambda^{-1}\right)\right]^n A_g L_s^{-n} W_s^{n+1}, \tag{12}$$

where n is the Nye-Glen flow law exponent, A_g is the Nye-Glen flow law coefficient, L_s is the length of the buttressing ice shelf, and W_s is the width of the ice shelf. In this grounding line flux approximation, $\beta = n+1 = 4$ and thus Q_g has a strongly nonlinear dependence on local ice thickness. In the limit that the ice shelf primarily loses mass through basal melting

$$\Omega = (n+1)^{-\frac{1}{n+1}} \left[\rho_i g \left(1 - \lambda^{-1}\right)\right]^{\frac{n}{n+1}} A_g^{\frac{1}{n+1}} W_s \left(-\frac{\dot{m}}{2}\right)^{\frac{n}{n+1}}, \tag{13}$$

where $\dot{m}$ is the basal melt rate (with the convention that $\dot{m} < 0$ indicates melting) and $\beta = 1$. These particular forms of the $Q_g(h_g)$ relationship allow us to understand how changes in the ice shelf cause changes in the thickness and grounding line position of a marine-terminating glacier (see section 4). However, we can equally well use the $Q_g(h_g)$ relationships derived in other studies (Schoof, 2007a; Schoof et al., 2017; V. C. Tsai et al., 2015). This flexibility of assumptions is one of the benefits of using a low-order model.

Asymptotic approximations for Q_g are not only valid for steady state glaciers but also describe the leading order time-dependent evolution of a bulk glacier (as in equation (1)) when the grounding region is close to

a steady state. This condition will be satisfied most of the time, because the grounding region adjusts on a very fast time scale when compared to the rest of bulk glacier. Mathematically, these adjustment terms enter as higher-order correction terms in the evolution equation of the grounding region (see, e.g., equation 3.37 in Schoof, 2007a). Indeed, previous studies (Drouet et al., 2013; Schoof, 2007b) and section 2.2 of this paper, show that when the ice sheet is reasonably close to a steady state, such quasi-steady approximations to the grounding line flux compare favorably to high-order numerical models of transient grounding line evolution. That being said, the very fast adjustment time scale described in Schoof (2007a) is not necessarily resolved by the two-stage model in this study.

2.2. Comparison to Flowline Model

In this section, we compare the simulated response of a marine-terminating glacier to external forcing in our two-stage model with a spatially extended glacier model. This comparison is helpful in determining how well the simplified dynamics of the two-stage model emulate a more complex model in terms of predicting response to a range of different forcing amplitudes and time scales. We use a flowline model (similar to what is described in Robel et al., 2014) with buttressing, a Weertman basal sliding law and fine horizontal resolution (∼100 m) near the grounding line. Velocity is solved from the following momentum balance and boundary conditions:

$$\frac{\partial}{\partial x}\left(2hA_g^{-\frac{1}{n}}\left|\frac{\partial u}{\partial x}\right|^{\frac{1}{n}-1}\frac{\partial u}{\partial x}\right)=\rho_i g h\frac{\partial h}{\partial x}+Cu^m \tag{14}$$

$$u(x=0)=0 \tag{15}$$

$$\left[2A_g^{-\frac{1}{n}}h\left|\frac{\partial u}{\partial x}\right|^{\frac{1}{n}-1}\frac{\partial u}{\partial x}\right]_{x=L}=\frac{1}{2}\rho_i g\left(1-\frac{\rho_i}{\rho_w}\right)\theta h(L)^2, \tag{16}$$

where θ is a dimensionless buttressing parameter. In this spatially extended model, ice flux is not prescribed at the grounding line but arises from the formation of the grounding zone boundary layer, as described by Schoof (2007a). The ice shelf is not explicitly simulated, but the buttressing effect is reproduced through modification of the stress boundary condition at the grounding line by buttressing parameters θ (Haseloff & Sergienko, 2018; Schoof, 2007b). Ice thickness changes through advection and surface mass balance,

$$\frac{\partial h}{\partial t}+\frac{\partial}{\partial x}(uh)=P, \tag{17}$$

and reaches flotation at the grounding line

$$h(L)=-\lambda b(L). \tag{18}$$

This numerical approach has been shown to accurately simulate marine-terminating glacier velocity and grounding line dynamics in previous studies (Robel et al., 2014; Schoof, 2006, 2007b).

To facilitate comparison to this flowline model, we use a grounding line flux expression in the two-stage model given in Schoof (2007a), where $\beta=\frac{m+n+3}{m+1}$ and $\Omega=\left[A_g\left(\rho_i g\right)^{n+1}\left(\theta(1-\lambda^{-1})\right)^n(4^nC)^{-1}\right]^{\frac{1}{m+1}}$. We bring both models to a stable equilibrium state on a downward sloping (prograde) bed, with a constant surface mass balance and other parameters specified in Table 1. In both the two-stage and flowline models, the resulting equilibrium is a glacier of approximately 2,200-m average thickness (H) with a grounding line 445 km from the ice divide (L). We then perform simulations (Figure 2) where stochastic interannual variability (P') is added to the time-averaged surface mass balance ($\bar{P}$). The random year-to-year variations in surface mass balance are drawn from a Gaussian normal distribution with mean zero and standard deviation that is 1/3 of the time-average surface mass balance. In both the two-stage and flowline models, we simulate the glacier variability forced by the same time series of noisy surface mass balance (Figure 2a), over 3×10^6 years, to obtain stationary statistical measures of the glacier variability. These stochastic-forcing simulations are a useful way to sample the response function for the marine-terminating glacier across a large range of frequencies.

White-noise forcing is the application of random perturbations to a model, drawn from a Gaussian distribution, and not depending on previous system state or perturbations. White-noise forces a system equally at all time scales greater than or equal to the time scale at which the perturbations are applied. We use such white-noise forcing (Figure 2a) to perturb the two-stage and flowline glacier systems at every yearly time step, and integrated using the Euler-Maruyama method. Thus, in our system, white-noise forces the glacier at time scales ranging from a year to tens of millennia. Figure 2 compares the simulated stochastic grounding line

Table 1
Parameters Used in Comparison Simulations in Section 2.2

Parameter	Description	Value
A_g	Nye-Glen law coefficient ($Pa^{-n} \cdot s^{-1}$)	4.22×10^{-25}
b_0	Ice divide bed height (m)	−100
b_x	Prograde bed slope	1×10^{-3}
C	Basal friction coefficient ($Pa \cdot m^{-1/n} \cdot s^{1/n}$)	7.624×10^6
g	Acceleration due to gravity (m/s^2)	9.81
m	Weertman friction law exponent	1/3
n	Nye-Glen law exponent	3
$\bar{P}$	Time-averaged accumulation rate (m/year)	0.3
σ_P	Accumulation rate variance (m/year)	0.1
α	Interior ice flux thickness exponent	7
γ	Interior ice flux length exponent	3
θ	Buttressing parameter	0.6
Δt	Time step (year)	1
ρ_i	Ice density (kg/m^3)	917
ρ_w	Seawater density (kg/m^3)	1,028

response across these time scales in the flowline model (black line) and the two-stage model (red line). The two-stage model simulates departures of the grounding line from its equilibrium position ($y = 0$ in Figure 2b) that are within 10% of the flowline model. Without having to tune any parameters, the structure of the autocorrelation function, power spectrum, and phase (Figures 2c–2e) are broadly similar between the two-stage and flowline models. Perhaps the most notable difference is that the two-stage model simulates less variability at very short time scales (a few decades) than the flowline model (Figure 2d). In the flowline model, variability in the surface mass balance near the grounding zone propagates to the grounding line on time scales of years to decades and the grounding zone adjusts on a similarly fast time scale (as shown in Schoof, 2007a and discussed in section 2). Since advection can only occur between the two zones in the two-stage model (which has a time scale of decades to centuries, see section 3), the fastest advection time scales are not well represented in the power spectral density and lagged autocorrelation function of the two-stage model (Figures 2c and 2d). This lack of variability at short time scales also leads to a lower standard deviation of fluctuations in the two-stage model than in the flowline model (by about 20%, see discussion in section 4.3). Additionally, the phase of the grounding line response at high frequencies (Figure 2e) is closer to 180° (indicating that surface mass balance forcing precedes the grounding line response) in the two-stage model than the flowline model, which remains between 90° and 120° at these frequencies. The phase of stochastic variations in the flowline model at high frequencies are the superposition of signals arriving at the grounding line from various locations throughout the glacier, and thus we should expect the combined grounding line response to be less than exactly out of phase (180°). In the two-stage model, the phase lag of signals at the grounding line are the result of a single advective time scale from the interior zone to the grounding zone. In practical terms, the two-stage model appears as a low-pass filter of the flowline model, with small interannual fluctuations in grounding line positions smoothed out relative to the flowline model. Despite these discrepancies, it is readily apparent in both models that the amplitude of variability at long time scales greatly exceeds variability occurring at subcentennial time scales (Figure 2d). Indeed, more than 99% of the total variability (measured as the integral over the power spectral density in Figure 2d) occurs at frequencies in which the two-stage and flowline models are consistent. Consequently, we conclude that the two-stage model successfully emulates the dynamics which produce the largest amplitude excursions of grounding line position in the flowline model.

The choice of a two-stage model is also indicated by fitting the time series of simulated grounding line position from the flowline model with an autoregressive model of arbitrary order (the Box-Jenkins method, see Box et al., 2015). We find that the flowline model can be well described by a second-order (AR(2)) regressive process governed by two widely separated time scales, 8300 years and 70 years, for the parameters in Table 1 (and for a range of other parameters, as we will show in section 3). Increasing the number of stages in the simple model (i.e., an arbitrary AR(p) model with $p > 2$) does improve the fit to the full flowline model by less than

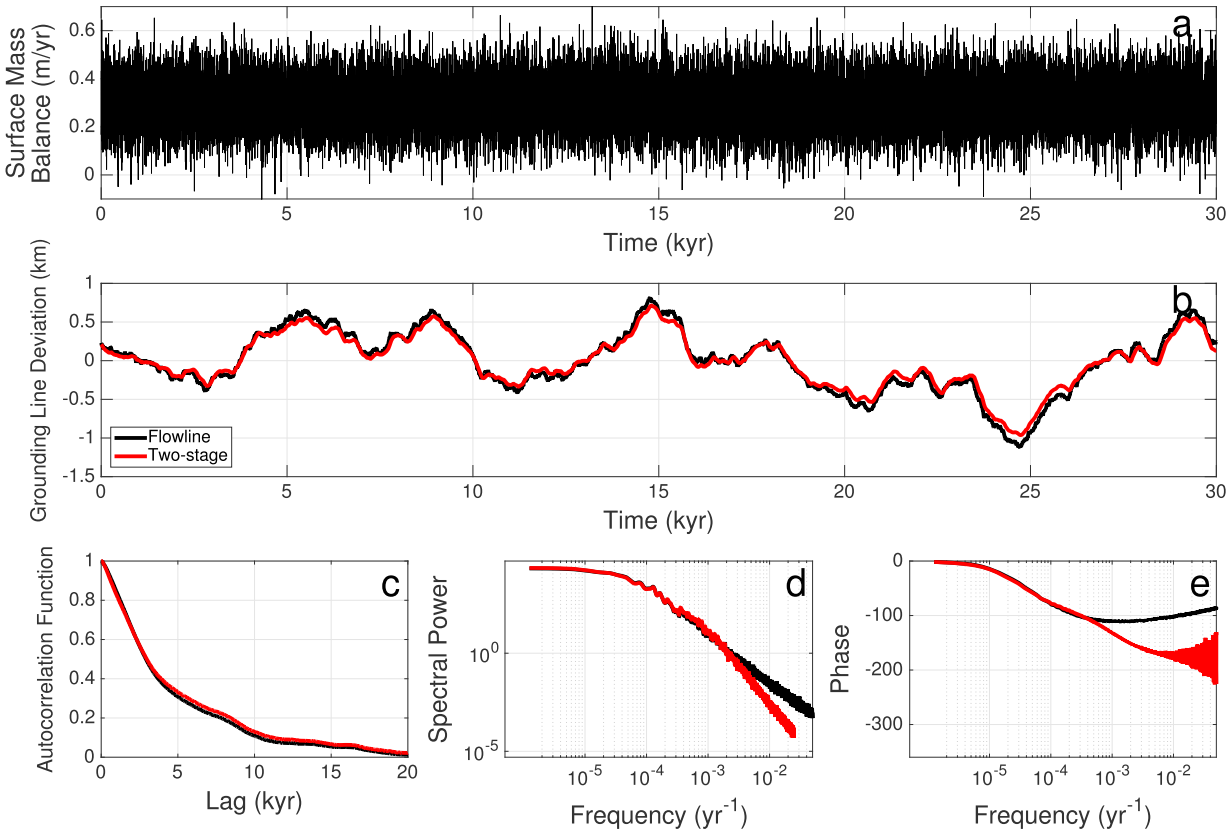

Figure 2. Comparison between two-stage (red line) and flowline (black line) simulations of grounding line variability due to white noise in surface mass balance. (a) Surface mass balance forcing (same for both models). (b) Simulated grounding line deviation from stable equilibrium position. 30-kyr time series taken from a 3000-kyr simulation. (c) Autocorrelation as a function of time lag. (d) Spectral power density as a function of frequency calculated via Welch's method with a window 1/30 the length of the total time series (10^5 years in this case). (e) Phase of grounding line position with respect to forcing in surface mass balance as a function of frequency.

1% (as judged by the Akaike Information Criterion for evaluating model quality). However, such an increase in complexity of the simple model does not improve our understanding of the dynamics of grounding line variability and hinders the straightforward analytical characterization of system dynamics that we describe in the coming sections.

3. Characteristic Time Scales

A complex numerical model can predict the response of a marine-terminating glacier to forcing under a variety of assumptions that are specific to that single glacier. Instead, with a simple model and fewer glacier-specific assumptions, we can derive the generic response of marine-terminating glaciers to forcing and understand the processes which control this response. This generic response is characterized by time scales and magnitudes of glacier change (or *sensitivities*). A system, such as our two-stage model for a marine-terminating glacier that is linearized about a stable equilibrium can be described more succinctly (and physically) by considering the time scales and sensitivities that govern the transient response to perturbations away from equilibrium. Such an approach is considerably more difficult in systems with many degrees of freedom.

We start by assuming that the two prognostic variables in the two-stage model, spatially averaged ice thickness H, and grounding line position L, are composed of a stable equilibrium state ($\bar{H}$, $\bar{L}$) and departures from this state (H', L') that are not necessarily stochastic fluctuations (rather deterministic functions of time)

$$H = \bar{H} + H' \tag{19}$$

$$L = \bar{L} + L'. \tag{20}$$

We assume that the departures are small compared to the stable equilibrium states ($H' \ll \bar{H}$, $L' \ll \bar{L}$). We can then substitute these expressions into the two-stage model (equations (7) and (8)), expand, and drop all terms that are higher than first order in H' and L'

$$\frac{\partial \bar{H}}{\partial t} + \frac{\partial H'}{\partial t} = P - \frac{\bar{Q}_g}{\bar{L}} - \frac{\bar{H}}{\bar{h}_g \bar{L}} \left(\bar{Q} - \bar{Q}_g\right) + A_H(\bar{H}, \bar{L})H' + A_L(\bar{H}, \bar{L})L' \tag{21}$$

$$\frac{\partial \bar{L}}{\partial t} + \frac{\partial L'}{\partial t} = \frac{1}{\bar{h}_g} \left(\bar{Q} - \bar{Q}_g\right) + B_H(\bar{H}, \bar{L})H' + B_L(\bar{H}, \bar{L})L', \tag{22}$$

where A_H, A_L, B_H, and B_L are the strengths of linearized feedbacks in the glacier system (expressions given in the supporting information). The strengths of these individual feedbacks are a function of the equilibrium glacier state ($\bar{H}, \bar{L}$). A_H is the magnitude of changes in interior ice flux due to changes in average ice thickness (H). A_L is the magnitude of changes in grounding line ice flux (Q_g) and grounding zone ice flux difference ($Q - Q_g$) due to changes in grounding line position (L). B_H is the magnitude of changes in interior ice flux due to changes in grounding line ice thickness ($\frac{Q}{h_g}$). B_L is the magnitude of changes in grounding zone ice flux divergence ($\frac{Q-Q_g}{L}$) due to changes in grounding line position (L).

When a stable equilibrium exists for a given glacier, $\frac{\partial \bar{H}}{\partial t}$ and $\frac{\partial \bar{L}}{\partial t}$ are by definition zero and the equilibrium terms (not involving departures from equilibrium) on the right-hand side of equations (21) and (22), which reflect the balance of stable equilibrium, sum to zero. This leaves a linear system of equations for departures in ice thickness (H') and grounding line position (L') and their associated feedbacks

$$\frac{\partial H'}{\partial t} = A_H(\bar{H}, \bar{L})H' + A_L(\bar{H}, \bar{L})L' \tag{23}$$

$$\frac{\partial L'}{\partial t} = B_H(\bar{H}, \bar{L})H' + B_L(\bar{H}, \bar{L})L'. \tag{24}$$

Generally, the solution to such a linear system of equations (23) and (24) is

$$L'(t) = C_S e^{-\frac{t}{T_F}} + C_L e^{-\frac{t}{T_S}} \tag{25}$$

where the eigenvalues of the system of equations are $-T_F^{-1}$ and $-T_S^{-1}$. These two exponential functions correspond to two characteristic time scales of adjustment in the marine-terminating glacier. Put another way, the eigenvalues of the linearized system quantify the adjustment rate and their sign determines the stability of the two-stage model (as in a linear stability analysis). If at least one of these eigenvalues is positive, there is no stable equilibrium, causing perturbations to grow rather than dissipate on at least one time scale. We discuss the nature of this instability in section 3.3.

After some further approximation (detailed in the supporting information), we can analytically derive the two time scales of the two-stage model

$$T_F = \frac{\bar{L}\bar{h}_g}{\bar{Q}(\alpha + \gamma)} - \frac{\bar{h}_g^2}{\bar{Q}_g \beta \lambda \bar{b}_x} \tag{26}$$

$$T_S = -\frac{\bar{H}\bar{h}_g\bar{L}^2}{\alpha T_F \bar{Q}} \left[\bar{Q} + \left(\frac{\beta \lambda b_x \bar{L}}{h_g}\right)\bar{Q}_g\right]^{-1}. \tag{27}$$

We calculate these time scales for a range of values of surface mass balance and bed slope (Figure 3). In general, there is a slow time scale (T_S) that is 1 to 2 orders of magnitude greater than the other time scale (T_F), which we call the fast time scale. For typical marine-terminating glacier thickness and time-averaged surface mass balance, the fast time scale ranges from decades to centuries and the slow time scale ranges from centuries to millennia (Figure 3a). Furthermore, as Figure 3 shows, these analytically derived time scales (solid lines) agree well with those determined from fitting the stochastic variability simulated in a spatially extended flowline model (crosses; described in section 2.2) with an autoregressive model through the Box-Jenkins fitting method (Box et al., 2015). As we discuss in section 2.2, there are other, even faster time scales of years to decades that contribute to advective adjustment of the glacier and grounding zone to external forcing and which are related to the fast adjustment time scale in the asymptotic analyses of Schoof (2007a) and Haseloff and Sergienko (2018). However, as we show these, very fast time scales play a lesser role in setting the transient glacier adjustment to external forcing.

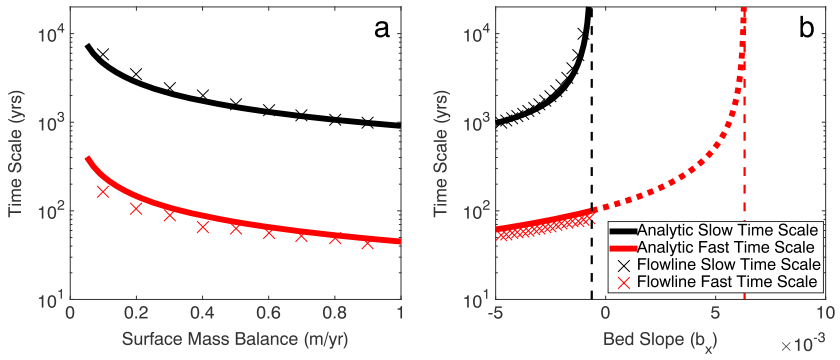

Figure 3. Characteristic time scales of the marine-terminating glacier response to external forcing. Thick lines are analytic predictions of fast (red) and slow (black) time scales from linearized two-stage model (equations (26) and (27)). Crosses are corresponding time scales calculated from an autoregressive-moving average (ARMA) fit to flowline model simulations using the Box-Jenkins method (Box et al., 2015). (a) Varying time-averaged surface mass balance ($\bar{P}$). Constant bed slope, $\bar{b}_x = -3 \times 10^{-3}$. (b) Varying bed slope at equilibrium state ($\bar{b}_x$). Constant time-averaged surface mass balance, $\bar{P} = 0.5$ m/year. Black dashed line is the instability threshold for the slow time scale (equation (33)). Thin red dashed line is the instability threshold for the fast time scale (equation (34)). At bed slope greater than the instability threshold for the slow time scale, there is no longer a stable equilibrium and so a thick dashed red line is based on the analytic prediction of fast time scale with an unstable fixed point.

3.1. Fast Time Scale

The physical processes that control the fast glacier response to perturbations can be understood from the form and origin of the terms in T_F (equation (26)). The first term on the right-hand side of equation (26) derives from the interior flux feedback to changes in ice thickness (A_H), and corresponds to the rate of interior advection ($\bar{Q}$) of anomalies in grounding line ice thickness. The second term is the rate at which ice flux divergence in the grounding zone changes as the grounding line migrates (B_L). At equilibrium, the surface mass balance is balanced by interior and grounding line flux: $\bar{P}\bar{L} = \bar{Q} = \bar{Q}_g$. We can then simplify the fast time scale as

$$T_F = \frac{\bar{h}_g}{\bar{P}} \left(\alpha + \gamma + 1 - S_T\right)^{-1}. \tag{28}$$

where

$$S_T = 1 + \frac{\beta\lambda\bar{b}_x\bar{L}}{\bar{h}_g}, \tag{29}$$

is a stability parameter that is typically $\mathcal{O}(1)$ and negative for sufficiently prograde bed slopes (downward sloping in the direction of flow, or $\bar{b}_x < 0$). On prograde slopes ($b_x < 0$) the terms in T_F have the same sign, and so the fast time scale is set by the largest term, $\alpha + \gamma \approx 10$ (where $\alpha + \gamma \gg \beta\lambda\bar{b}_x\bar{L}\bar{h}_g^{-1}$). This implies that the primary control on the fast time scale is the rate of advective adjustment of grounding zone ice thickness. Thus, the fast time scale may be approximated as

$$T_F \approx \frac{\bar{h}_g}{\bar{P}(\alpha + \gamma)}. \tag{30}$$

In a stable equilibrium, this rate of advective adjustment is proportional to $\frac{\bar{h}_g}{\bar{P}}$, which is the *reservoir time scale* on which ice volume in the grounding zone region is replaced by the surface mass balance. Though this approximation is not explicitly dependent on processes occurring in the ice shelf, their influence does enter through the way in which they contribute to setting the equilibrium grounding line ice thickness ($\bar{h}_g$). The reservoir time scale (generically $\frac{h}{P}$) is also discussed in previous studies of the glacier response to forcing (Harrison et al., 2003; Jóhannesson et al., 1989; Nye, 1960, 1963a, 1963b, 1965), which found that even if we did not know the glacier velocity or internal dynamics all that well (as assumed in Harrison et al., 2003), we could use the observed geometry to understand the glacier sensitivity through this reservoir time scale. Fortunately, recent advances in grounding line dynamics have allowed us to explicitly derive the nondimensional parameter that modifies this reservoir time scale (the unknown parameter *f* in Jóhannesson et al., 1989, and $\alpha + \gamma \approx 10$ in equation (30). This nondimensional parameter quantifies how the particular glacier dynamics may also play a role (in addition to the geometry) in setting the glacier response time scales. In these

ways, our approach of studying glacier departures about an equilibrium state explicitly links glacier geometry to ice dynamics and allows us to make progress from previous approaches to understanding glacier response time scales.

3.2. Slow Time Scale

The slow glacier response to forcing (equation (27)) is a function of the fast time scale, the magnitude of the interior ice flux feedback, and the grounding zone flux divergence feedback. At equilibrium, the time-averaged surface mass balance is balanced by interior and grounding line flux ($\bar{P}\bar{L} = \bar{Q} = \bar{Q}_g$), and so the slow time scale simplifies

$$T_S = -\frac{\bar{H}\bar{h}_g}{\alpha T_F \bar{P}^2 S_T}. \tag{31}$$

When multiplied by the grounding zone ice flux (Q_g), the stability parameter S_T tracks the difference between the rates of glacier advective adjustment and extension of the glacier by grounding line migration. For typical stable grounding lines (where T_F is approximation given by equation (30), the slow time scale can be approximated as

$$T_S \approx \frac{\bar{H}\left(1 + \frac{\gamma}{\alpha}\right)}{\bar{P}S_T}, \tag{32}$$

which is millennia for typical accumulation rates and ice thicknesses (see Figure 3). Physically, this slow time scale corresponds to the rate at which perturbations in ice thickness advected into the grounding zone are dissipated by differences in advective and extensional adjustment. The slow time scale includes the reservoir time scale for the entire glacier, $\frac{H}{P}$, though the explicit inclusion of glacier velocity in our model leads to modification by the stability parameter (S_T) and the interior ice flux exponents (α, γ). As a result, the slow time scale is longer than the fast time scale by 1 to 2 orders of magnitude. Indeed this response time of centuries to millennia for stable marine-terminating glaciers is more similar to that derived numerically in the idealized outlet glacier modeling study of van der Veen (2001). As the bed slope becomes shallower, S_T decreases, causing the slow time scale to increase, before eventually becoming negative, as we discuss in the next section.

3.3. Instabilities of Time Scales

Weertman (1974) first established that ice sheet grounding lines are unstable on retrograde bed slopes (upward sloping in the direction of flow, or $\bar{b}_x > 0$), commonly referred to as the *marine ice sheet instability*. Subsequent work has found that this instability extends to flat and shallow prograde beds (Schoof, 2012), though other factors may play a role in modulating this stability threshold in bed slope (Gomez et al., 2010; Gudmundsson et al., 2012; Jamieson et al., 2012) and the rate of grounding line migration under instability (Brondex et al., 2017). In our model, this instability occurs when the slow time scale becomes negative ($-1/T_S \geq 0$ in equation (25) as bed slope flattens (b_x is negative and increasing) and S_T becomes positive. This happens at

$$\bar{b}_x^{*S} = -\frac{\bar{h}_g}{\beta\lambda\bar{L}}, \tag{33}$$

which corresponds to a shallow prograde bed slope (black dashed line in Figure 3b). Exactly at this stability threshold, the slow time scale diverges, which physically corresponds to a glacier at neutral stability where perturbations to glacier state are neither damped or amplified by the glacier response (on this slow time scale). This stability threshold is also consistent with the linear stability condition derived by Schoof (2012), in which grounding lines resting on retrograde and shallow prograde bed slopes are unstable to perturbations. We have written the stability criterion as a function of equilibrium glacier geometry (instead of surface mass balance, as in Schoof, 2012), which is, in part, set by the surface mass balance ($P\bar{L} = \bar{Q}_g$). Past this threshold in bed slope, the slow time scale is no longer defined since the stable equilibrium glacier state no longer exists.

Conversely, the fast time scale remains finite and defined for bed slopes flatter and more retrograde than $\bar{b}_x^{*S}$. The fast time scale increases until it also diverges ($T_F \to \infty$) and then becomes negative at a moderately steep retrograde slope of

$$\bar{b}_x^{*F} = \frac{\bar{h}_g}{\beta\lambda\bar{L}}(\alpha + \gamma). \tag{34}$$

Above this threshold, the decay rate associated with the fast time scale is positive ($-1/T_F \geq 0$ in equation (25). As bed slope increases, changes in grounding line position cause less adjustment through grounding line flux

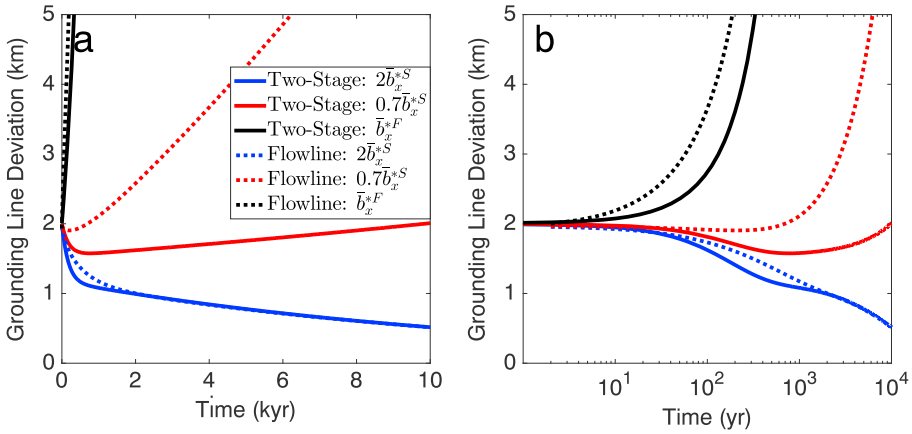

Figure 4. Grounding line migration from an initially perturbed state (2 km from equilibrium) simulated in two-stage (solid lines) and flowline (dashed lines) models for a range of bed slopes at the grounding line. The blue line is the stable grounding line response for a prograde bed slope steeper than the slow stability threshold ($\bar{b}_x = -5.1 \times 10^{-4}$). The red line is the grounding line response for a prograde bed slope shallower than the slow stability threshold ($\bar{b}_x = -1.8 \times 10^{-4}$). The black line is the unstable grounding line response for a retrograde bed slope at the fast stability threshold ($\bar{b}_x^{*F} = 2.6 \times 10^{-3}$). (a) Plotted in linear coordinates. (b) Plotted with logarithmic coordinates on the *x* axis.

(i.e., the third term on the right-hand side of equation (26) decreases in magnitude). Eventually, perturbations in the grounding line position can no longer be accommodated by changes in ice advection to the grounding zone and the fast time scale becomes negative.

It is always the case that $\bar{b}_x^{*S} < \bar{b}_x^{*F}$ or that as bed slope becomes shallower, slow grounding line dynamics become unstable before fast grounding line dynamics. This implies that there is a wide range of intermediate shallow bed slopes ($\bar{b}_x^{*S} < \bar{b}_x < \bar{b}_x^{*F}$, the region between the thin black and red dashed lines in Figure 3b) for which the grounding line is unstable on slow time scales but stable on fast time scales. We demonstrate the consequence of these distinct stability thresholds in Figure 4, which shows two-stage (solid) and flowline (dashed) model simulations of the grounding line migration from an initially perturbed state (2 km) for several different bed slopes. A grounding line on a steep prograde bed slope (blue lines, for which $\bar{b}_x < \bar{b}_x^{*S}$) exhibits stable dissipative behavior (i.e., it returns to equilibrium) at both short and long time scales. For strongly retrograde bed slopes (black lines, for which $\bar{b}_x = \bar{b}_x^{*F}$), the grounding line is unstable on both fast and slow time scales. In such a scenario, even short-lived departures in the glacier state from equilibrium immediately grow, rather than decay. For shallow prograde or shallow retrograde bed slopes (red lines, for which $\bar{b}_x^{*S} < \bar{b}_x < \bar{b}_x^{*F}$) the perturbed grounding line position is nearly stagnant or retreating toward equilibrium (at $y = 0$) on fast time scales (centuries) but is unstable on long time scales (millennia). When the grounding line is unstable and the glacier is strongly out of equilibrium, asymptotic approximations for the grounding line flux (equation (11)) become less accurate (Schoof, 2007b). This is apparent from the increasing departure between the unstable retreat simulated in the flowline and the two-stage model on time scales of millennia. Nonetheless, both models indicate that there is a range of bed slopes for which a perturbed grounding line may exhibit stable behavior on the short term, but is ultimately unstable in the long term. This nonmonotonic grounding line response to a perturbation occurs because marine-terminating glaciers have more than one time scale both in the two-stage and flowline models, which become unstable at different bed slope thresholds. We call this scenario, when the slow time scale is unstable, but the fast time scale is stable, the *slow* marine ice sheet instability. For sufficiently steep retrograde slopes the grounding line is unstable at both slow and fast time scales. We call this the *fast* marine ice sheet instability.

Many glaciers in Greenland and West Antarctica are (likely) undergoing an unstable retreat over steep retrograde bed slopes at rates of kilometers per year (Joughin et al., 2008; Park et al., 2013; Scheuchl et al., 2016). In this section, we determined the conditions under which this instability occurs (equations (34) and (33)) and show qualitatively that rapid glacier change may occur due to the fast marine ice sheet instability. However, we cannot easily extend our linear analysis of marine-terminating glacier response to quantitatively

determine the transient rate of glacier change on retrograde or shallow prograde bed slopes since the lack of a stable equilibrium causes the linearity of the glacier response to be a bad approximation. Future work may consider using nonequilibrium approaches for systems near instabilities (Nicolis & Nicolis, 1981; Suzuki, 1977) to assess the behavior of marine-terminating glaciers on retrograde bed slopes.

4. Sensitivity to Forcing

Observations indicate that marine-terminating and tidewater glaciers are undergoing strongly heterogenous changes (Brinkerhoff et al., 2017; Csatho et al., 2014; Felikson et al., 2017; Post & Motyka, 1995). This heterogeneity may be caused by factors that vary from one glacier to another, such as forcing rate, glacier state, bed topography, or time scale of response. Our challenge is to understand how the magnitude and rate of the glacier response to external forcing is controlled by these various factors. Having derived the characteristic glacier response time scales, we have already solved half the problem of the time-dependent glacier response to forcing. In this section, we will solve the second half of the problem, by deriving the total and transient sensitivity of marine-terminating glacier state to different types of external forcing.

4.1. Total Fractional Sensitivity

In this section, we derive the sensitivity of marine-terminating glaciers to forcing by extending the linearization of the two-stage model to time-dependent perturbations in external forcing parameters. To demonstrate the approach, we start by decomposing P (the spatially averaged surface mass balance) into time-averaged and perturbed components

$$P = \bar{P} + P' \tag{35}$$

which leads to an expanded form of linear equation (23)

$$\frac{\partial H'}{\partial t} = A_H(\bar{H}, \bar{L})H' + A_L(\bar{H}, \bar{L})L' + P' \tag{36}$$

which now includes glacier feedbacks to perturbations in surface mass balance. For a change in surface mass balance (P'), we calculate the magnitude of changes in glacier state (H' and L') once the system has reached a new steady state, which occurs when $\frac{\partial H'}{\partial t} = 0$ and $\frac{\partial L'}{\partial t} = 0$ in equations (25) and (37) (derived in detail in the supporting information)

$$\frac{H'}{\bar{H}} = \frac{1}{\alpha S_T}\left(\frac{\beta\lambda\bar{b}_x\bar{L}}{\bar{h}_g} - \gamma\right)\frac{P'}{\bar{P}} \tag{37}$$

$$\frac{L'}{\bar{L}} = -\frac{1}{S_T}\frac{P'}{\bar{P}}. \tag{38}$$

These are the fractional sensitivities of average glacier thickness ($H'/\bar{H}$) and grounding line position ($L'/\bar{L}$), to a fractional change in surface mass balance ($P'/\bar{P}$).

We can also derive the glacier sensitivity to changes in the observable ice shelf parameters that go into Ω. For a glacier strongly buttressed by an ice shelf that primarily loses ice through calving (Ω in equation (12), we derive the fractional glacier sensitivity to a fractional change in the ice shelf length ($L_s'/\bar{L}_s$)

$$\frac{H'}{\bar{H}} = -\frac{(\gamma+1)n}{\alpha S_T}\left(\frac{L_s'}{\bar{L}_s}\right) \tag{39}$$

$$\frac{L'}{\bar{L}} = -\frac{n}{S_T}\left(\frac{L_s'}{\bar{L}_s}\right). \tag{40}$$

These sensitivities show the extent of grounding line retreat and interior ice thinning that would be expected after, for example, the detachment of an iceberg from an ice shelf that reduces the buttressing ice shelf length (assuming all parts of the ice shelf contribute equally to buttressing). Alternately, we consider an ice shelf that strongly buttresses a glacier and loses mass entirely through basal melting (Ω in equation (13). We then derive the fractional glacier sensitivity to fractional changes in basal melt rate (where $\dot{m} < 0$ indicates melting)

$$\frac{H'}{\bar{H}} = \frac{(\gamma+1)n}{\alpha(n+1)S_T}\left(\frac{\dot{m}'}{\bar{\dot{m}}}\right) \tag{41}$$

$$\frac{L'}{\bar{L}} = \frac{n}{(n+1)S_T}\left(\frac{\dot{m}'}{\bar{\dot{m}}}\right). \tag{42}$$

The fractional sensitivities of ice thickness and grounding line position (equations (37)–(42)) indicate some general rules about the expected magnitude of the glacier response to external forcing. The fractional change in glacier state from equilibrium can be approximated as proportional to the fractional change in climate forcing ($\frac{P'}{\bar{P}}$, $\frac{\dot{m}'}{\bar{\dot{m}}}$) or a property of the buttressing ice shelf ($\frac{L'_s}{\bar{L}_s}$). This proportionality is generally modulated by the inverse of the stability parameter (S_T), and the strength of the nonlinearity of the forcing process (1 for surface mass balance, $-n$ for ice shelf length in equation (12), and $\frac{n}{n+1}$ for basal melting rate in equation (13). For ice thickness, the strength of the nonlinearity in interior ice flux (α, γ) also enters. As the bed slope becomes shallower, S_T decreases in magnitude, and a given magnitude of external forcing will result in a larger change in glacier thickness and grounding line position.

We consider an illustrative example of a marine-terminating glacier that is $\bar{L} = 200$-km long, $\bar{h}_g = 1{,}000$ m thick at the grounding line, and undergoes a 5% decrease in surface mass balance. Using equation (38) we would predict that on a prograde bed slope of $\bar{b}_x = -3\times10^{-3}$, the glacier would retreat by 3% of its length. However, if the prograde bed slope is twice as shallow ($\bar{b}_x = -1.5\times10^{-3}$), the glacier would instead retreat by 14% of its length, albeit over a longer time scale. Alternately, for the same glacier, a 5% decrease in buttressing ice shelf length causes the glacier to retreat by 9% of its length on a $\bar{b}_x = -3\times10^{-3}$ prograde slope and 43% of its length on a $\bar{b}_x = -1.5\times10^{-3}$ prograde slope. The nonlinear dependence of the grounding line flux on ice shelf length leads to a more sensitive response to perturbations than is the case for perturbations in surface mass balance.

Overall, the sensitivities we derive depend only on glacier state, nonlinearity in glacier dynamics, and the time-averaged value of the forcing parameter. The magnitude of grounding line changes on the slow time scale alone can also be simulated by a one-stage counterpart of the two-stage model of this study (where we assume that $PL = Q$):

$$\frac{\partial L}{\partial t} = \frac{1}{h_g}\left(PL - Q_g\right). \tag{43}$$

Equilibrium occurs when surface mass balance is balanced by grounding line flux ($\bar{P}\bar{L} = \bar{Q}_g$). Since a change in surface mass balance must be balanced by a change in grounding line flux, the sensitivity of the grounding line position will be the same in our two-stage model, its one-stage counterpart (equation (43)), and a range of higher-order models. Indeed, we find that the sensitivities derived in this section match those calculated in the flowline model described in section 2.2, to the extent that its modeled steady state grounding line flux matches the grounding line flux expression used in the two-stage model (equation (11)). We similarly expect that other high-order models that accurately simulate grounding line flux will also match these sensitivities. In this way, these expressions for glacier sensitivity serve as useful first-order approximations for the glacier response that can be calculated without use of a complex ice sheet model.

4.2. Transient Response to Trends and Step Changes in Forcing

The glacier response to forcing is not instantaneous, but rather evolves in time. In this section we derive the transient grounding line migration in response to a trend or step change in external forcing. We then discuss the relative importance of forcing rate and the characteristic time scales in determining the rate of the glacier response to forcing.

We assume that the marine-terminating glacier begins at stable equilibrium with initial conditions

$$L'(t=0) = 0 \tag{44}$$

$$\left.\frac{dL'}{dt}\right|_{t=0} = 0. \tag{45}$$

We then apply a trend ($\dot{P}$) in surface mass balance (though the same general approach applies for a trend in any parameter), $P'(t) = \dot{P}t$. We solve for the time-dependent grounding line position in equations (36)

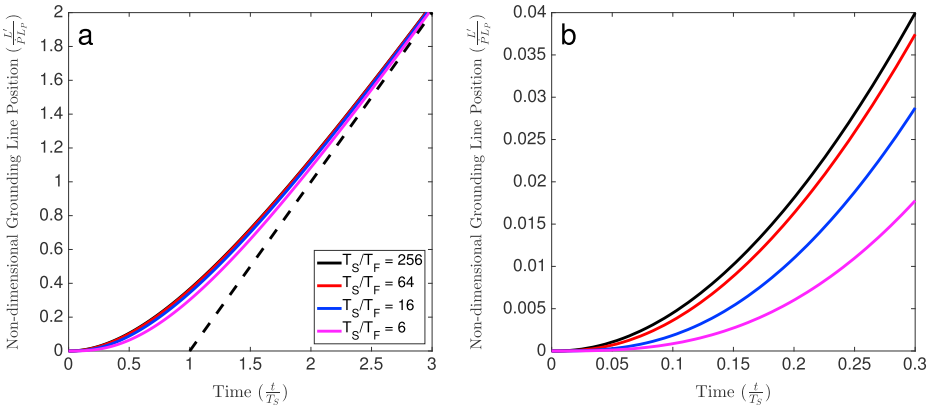

Figure 5. Response of grounding line position to a trend in surface mass balance (equation (46)) for different ratios between fast and slow time scales (T_S/T_F). Grounding line position (y axis) is nondimensionalized with $L'/\dot{P}L_P$. Time (x axis) is also nondimensionalized with $\frac{t}{T_S}$. (a) Shape of grounding line trend. Dashed black line is the long-term rate of grounding line migration forced by a trend in surface mass balance (equation (48)). (b) Zoomed version of panel (a), meant to highlight the different initial responses to a trend on the fast glacier time scale (T_F).

and (37) (linearized form of the two-stage model) using the method of undetermined coefficients (complete derivation in supporting information)

$$L'(t) = \dot{P}L_P T_S \left[\frac{1}{2}\left(1 - \frac{T_S - 2T_F}{\left(T_S^2 - 4T_S T_F\right)^{\frac{1}{2}}}\right) e^{-\frac{t}{T_F}} + \frac{1}{2}\left(1 + \frac{T_S - 2T_F}{\left(T_S^2 - 4T_S T_F\right)^{\frac{1}{2}}}\right) e^{-\frac{t}{T_S}} - 1 + \frac{t}{T_S} \right], \tag{46}$$

where $L_P = -\frac{\bar{L}}{S_T \bar{P}}$ is the grounding line sensitivity to perturbations in surface mass balance (which can be derived for other parameters from equations (38), (40), and (42). This solution is valid when $T_S > 4T_F$, which is true for a range of glacier conditions (Figure 3).

The transient grounding line evolution forced by a linear trend in surface mass balance and simulated in the flowline model is well approximated by equation (46) (not plotted). In Figure 5, we show that the shape of the glacier response only depends on the slow and fast time scales, when normalized by the trend rate in forcing and the sensitivity to forcing in a specific parameter ($\dot{P}L_P$). Since typically the slow time scale is much longer than the fast time scale (again, see Figure 3), we can make the simplification that the transient grounding line response to a trend is only dependent on the slow time scale

$$L'(t) = -\dot{P}L_P T_S \left[e^{-\frac{t}{T_S}} - 1 + \frac{t}{T_S} \right]. \tag{47}$$

Figure 5 shows that as T_S/T_F increases, the transient response converges quickly to this simplified response that only depends on the slow time scale.

After a sufficiently long period of time, the grounding line evolves at a constant rate set by the trend in forcing and the sensitivity (black dashed line in Figure 5a)

$$\left.\frac{\partial L'}{\partial t}\right|_{t>>T_S} = -\dot{P}L_P. \tag{48}$$

However, the grounding line migration rate remains relatively small in the time immediately after the onset of a trend (t), as long as $t \ll T_S$ (Figure 5b). Any reasonable estimate of T_S for a marine-terminating outlet glacier in Greenland or Antarctica will be at least 1,000 years (Figure 3), whereas the onset of significant anthropogenic forcing trends is estimated to be around 1880 (Intergovernmental Panel on Climate Change, IPCC, 2013). This implies that the current stable glacier changes being observed (not including unstable glacier retreat over retrograde slopes, which are discussed in section 3.3) are still close to the onset of the response functions in Figure 5. Hence, the initial glacier retreat over a prograde bed that is caused by industrial-era trends in climate occurs at an approximate rate,

$$\left.\frac{\mathrm{d}L'}{\mathrm{d}t}\right|_{t<<T_S} \approx -\dot{P}L_P \frac{t}{T_S}, \tag{49}$$

that is, a small fraction ($\frac{t}{T_S}$) of the long-term grounding line migration rate expected from a continuation of the industrial era trend in climate forcing (equation (48)). Put another way, if current rates of climate change continue, we would expect that the grounding line migration rate of stable marine-terminating glaciers will eventually accelerate to be many times (perhaps even an order of magnitude if $T_S > 1{,}000$ years) greater than current rates, even if the grounding line does not migrate into regions of retrograde or drastically different bed slope.

The response of the grounding line to a step change in forcing (of magnitude P') is similarly straightforward to derive, from equations (36), (37), and initial conditions (44) and (45), the transient solution is

$$L'(t) = -L_P P' \left[\left(\frac{T_F}{T_S - T_F} \right) e^{-\frac{t}{T_F}} - \left(\frac{T_S}{T_S - T_F} \right) e^{-\frac{t}{T_S}} + 1 \right], \tag{50}$$

with the fast and slow adjustment time scales mediating the grounding line response.

Observational records of marine-terminating glacier thickness and length tend to be short. Though reconstructions of local climate may be longer, climate trends can often be difficult to accurately estimate in the presence of interannual and subannual climate variability. This inability to precisely determine when a trend started can make it difficult to exactly pinpoint when a change in forcing begins (i.e., when $t = 0$ in equations (46) and (50). Consequently, uncertainty in the time of climate forcing onset ($t = 0$) leads to significant uncertainty in short- to medium-term projections of marine-terminating glacier change.

4.3. Stochastic Variability

Stochastic variability of marine-terminating glaciers will arise in the presence of internal variability in climate forcing. To identify the response of glaciers to climate changes, it is first necessary to understand the response of glaciers to stochastic climate variability. In this study, we consider white-noise perturbations in forcing parameters.

The linearized two-stage model equations (36) and (37) are discretized in time using a forward Euler-Maruyama method, implying an Itô formulation of the stochastic differential equation. Combining the two discretized equations, we derive a second-order autoregressive (AR(2)) model for the grounding line position

$$L_t = \left(2 - T_F^{-1}\Delta t - T_F^{-1}T_S^{-1}\Delta t^2\right) L_{t-\Delta t} + \left(-1 + T_F^{-1}\Delta t\right) L_{t-2\Delta t} - T_F^{-1}T_S^{-1}\Delta t^2 L_P P', \tag{51}$$

where P' is a Gaussian, white-noise process representing stochastic variability in surface mass balance at time scale Δt (throughout this study, we take $\Delta t = 1$ year). We then use the analytic variance of an AR(2) process found in Box et al. (2015) to derive the variance of the grounding line position. After some approximation (detailed in supporting information), the variance of the grounding line position can be expressed as

$$\sigma_L^2 = \frac{T_S \Delta t}{2} \left[\frac{\alpha T_F \bar{P} \bar{L}}{\bar{H} \bar{h}_g} \right]^2 \sigma_P^2 \tag{52}$$

where σ_P is the variance of the surface mass balance. All details of the above derivation are given in the supporting information.

For a typical marine-terminating glacier in Greenland, $\bar{H} \sim 1$ km, $\bar{Q}_g/\bar{h}_g \sim 1$ km/year, $T_S \sim 1{,}000$ years, and $T_F \sim 50$ (Figure 3) and interannual variability in surface mass balance (σ_P) is in the range 0.1–1 m/year (Fyke et al., 2014). These parameters suggest a range of $\sigma_L \approx 0.1$–5 km. This range is comparable to the few estimates that have been made of natural marine-terminating glacier variability (e.g., Bjørk et al., 2012; Hogg et al., 2016, though such estimates are typically made from short photographic or satellite records). It should also be noted that noisy forcing with interannual persistence (e.g., red noise) results in enhanced stochastic glacier variability (Mantelli et al., 2016; Roe & Baker, 2016), and so noise autocorrelation is important to consider when interpreting observations of glacier variability. Figure 6 demonstrates that, even with the simplifications inherent in the derivation of an analytic approximation of grounding line variability (solid line), equation (52) agrees with numerically calculated grounding line variability from a flowline model (crosses) to within 20%. The analytic prediction is systematically below the flowline model, because the two-stage model has muted fluctuations at high frequencies compared to the flowline model (though these high-frequency fluctuations typically have amplitude <100 m, see Figure 2b and section 2.2).

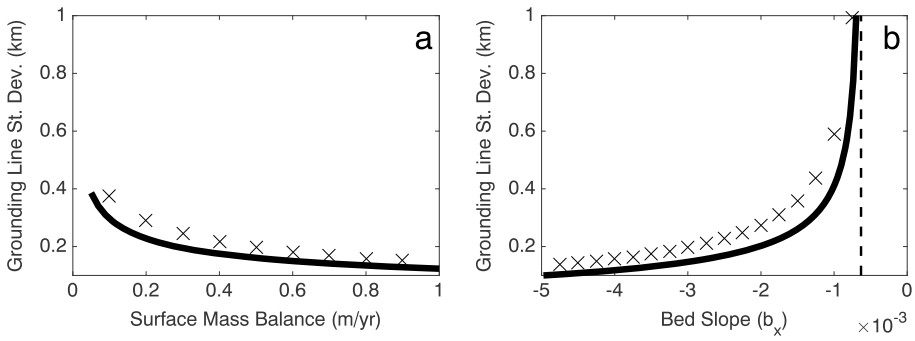

Figure 6. Standard deviation of grounding line position fluctuations in response to white-noise forcing in spatially averaged surface mass balance ($\sigma_P = 0.1$ m/year). Solid lines are analytic predictions of standard deviation of grounding line position (σ_L) from linearized two-stage model (equation (52)). Crosses are corresponding standard deviation calculated from flowline model simulations forced with white noise (e.g., Figure 2). (a) Varying time-averaged surface mass balance ($\bar{P}$). Constant bed slope, $\bar{b}_x = -3 \times 10^{-3}$. (b) Varying bed slope at equilibrium state ($\bar{b}_x$). Constant time-averaged surface mass balance, $\bar{P} = 0.5$ m/year. Black dashed line is the instability threshold for the slow time scale (equation (33)).

Stochastic grounding line variability (equation (52)) is dependent on both the short and fast time scales. Thus, as bed slopes become shallower and approach the slow time scale instability (equation (33)), the variance of grounding line position increases rapidly along with the slow time scale (Figure 6b). This increasing variance and decreasing rate of dissipation of fluctuations are hallmarks of *critical slowdown*, which is a generic feature of dynamical systems smoothly approaching bifurcations to instability (e.g., Lenton, 2011).

5. Nonlinearity of Noisy Processes Causes Grounding Line Retreat

In our two-stage model of a marine-terminating glacier, noise in surface mass balance (P') is additive because it directly perturbs the glacier thickness, but does not depend on the glacier state. On the other hand, noise in the coefficient of grounding line flux (Ω') is multiplicative because it perturbs the grounding line flux, which also depends on the grounding line position. In this section, we show that nonlinearity in a multiplicative noise process changes the time-averaged equilibrium state of a marine-terminating glacier.

In Figure 7, we compare the response of the two-stage glacier model to white-noise forcing in four different environmental parameters: surface mass balance (P), coefficient of grounding line flux (Ω), ice shelf length (L_s), and basal melt ($\dot{m}$). In each of these 60-kyr simulations, we simulate the grounding line response to forcing without noise in the first 20 kyr, with white noise of magnitude equal to 10% of the mean in the next 20 kyr, and with white noise of magnitude equal to 20% of the mean in the final 20 kyr. As we have seen previously in this study, when there is white noise in the spatially averaged surface mass balance (Figure 7a), the time-averaged grounding line position remains constant regardless of the magnitude of noise.

We also vary the magnitude of noise in the coefficient of grounding line flux (Ω'; Figure 7b). However, even though this is a multiplicative noise process, the time-averaged glacier state does not appear to depend significantly on the magnitude of the noise. This is because the state variable in the grounding line flux term, h_g, does not strongly vary when ice is thick at the grounding line, leading to rather weak state dependence. If instead ice was thinner at the grounding line (such as in a tidewater glacier), grounding line flux would be more sensitive to small changes in system state, thus leading to stronger state dependence.

In reality, noise does not occur in Ω directly, but rather in the various processes that contribute to Ω. The grounding line flux of a glacier buttressed by a calving-dominated ice shelf is a function of L_s^{-n} (equation (12)). We consider a scenario where the calving of icebergs from an ice shelf causes white-noise fluctuations in L_s (Bassis, 2011). The corresponding time-averaged grounding line position (Figure 7c, note the different y axis scale) is strongly a function of the magnitude of the forcing. Of all the forcing processes considered here, this shift in the time-averaged state is by far the largest (by more than 2 orders of magnitude). We can explain why this shift occurs by noting that when ice shelf length increases from its equilibrium value by 10%, grounding line flux decreases by 25%, and when ice shelf length decreases from its equilibrium value by 10%, grounding line flux decreases by 37%. Thus, though the distribution of noisy ice shelf length is symmetric, the corresponding distribution of noisy grounding line flux is asymmetric, leading to a shift in the time-averaged grounding

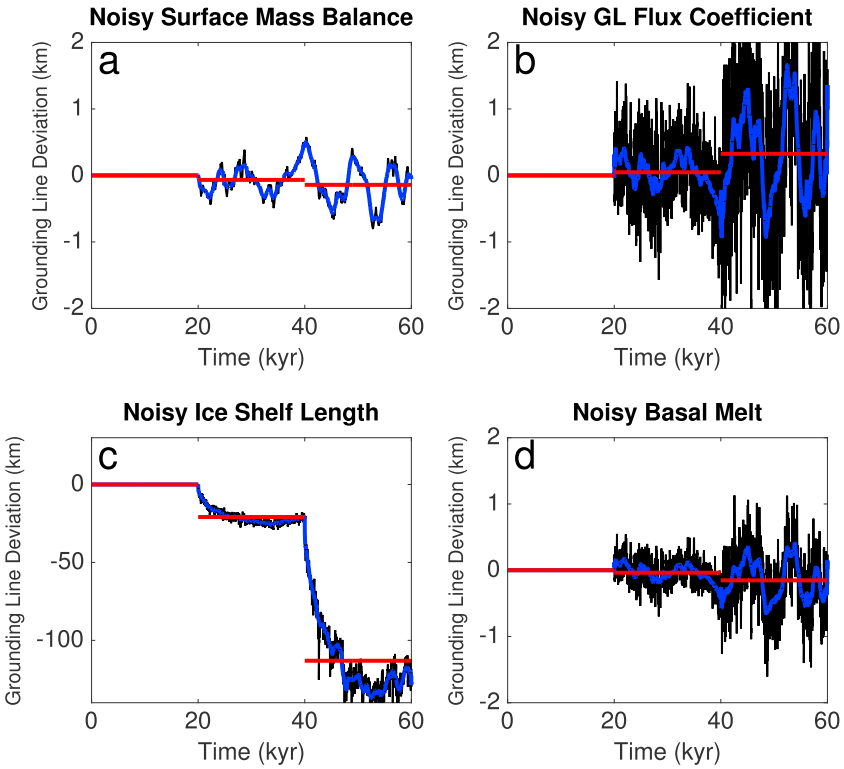

Figure 7. Grounding line deviation from equilibrium simulated in the two-stage model due to noise in different forcing parameters. Black line in all panels is year-to-year grounding line position simulated in two-stage model. Blue line is 1,000-year running average. Red line in all panels is average over time period of constant noise magnitude. 0-20 kyr in all simulations have no noise in forcing. In all simulations 20–40 kyr have noise with standard deviation equal to 10% of mean forcing value. In all simulations 40–60 kyr have noise with standard deviation equal to 20% of mean forcing value. (a) Noise in surface mass balance (P'). (b) Noise in grounding line flux coefficient (Ω'). (c) Noise in ice shelf length (L_s'). (d) Noise in ice shelf basal melt ($\dot{m}'$).

line flux and glacier state. Though we have assumed that the noise forcing of ice shelf length includes no persistence in time (white noise), it would be more realistic to simulate ice shelf calving with autocorrelation in time. This would lead to greater stochastic glacier variability (Mantelli et al., 2016; Roe & Baker, 2016) and perhaps an even larger shift in the time-averaged glacier state.

Such a dependence of the mean state on the magnitude of noise forcing is typically termed *noise-induced drift* and has been explored extensively (e.g., Penland, 2003). Noise-induced drift has also been noted previously in other nonlinear glacier models with other types of forcing (Hindmarsh & Le Meur, 2001; Mikkelsen et al., 2017). Our simulation of noisy calving-induced drift suggests that the character of calving events (i.e., size and recurrence time) may have a strong influence on the time-averaged glacier state. Consequently, ice sheet models may be strongly biased by parameterizing calving as a deterministic flux or by misrepresenting the nature of calving-induced noise in ice shelf length. Flexible stochastic approaches to simulate calving, such as Bassis (2011), are better suited to capturing the noise-induced retreat that we have identified here.

Haseloff and Sergienko (2018) have also derived a more general relationship between flux and ice thickness at the grounding line

$$\dot{m}\Omega^{\frac{1}{n}}L_s h_g^{\frac{n+1}{n}} = (Q_g + \dot{m}L_s)^{\frac{n+1}{n}} - Q_g^{\frac{n+1}{n}} \tag{53}$$

which includes the effect of both sub-ice shelf basal melting and ice shelf length on buttressing. We use this formula to find the grounding line flux in the presence of interannual noise in the ice shelf basal melt (similar to what is predicted by ocean models, e.g., Schodlok et al., 2012; Sciascia et al., 2013). We find that the white noise in basal melt has only a small effect on the time-average grounding line position (Figure 7d). This is likely due to the much weaker nonlinearity in basal melt rate ($\frac{n+1}{n} = \frac{4}{3}$).

6. Discussion

6.1. Observed Marine-Terminating Glacier Change

Observations indicate that many marine-terminating glaciers have retreated and thinned over the last several decades (Joughin et al., 2010; Moon et al., 2015; Pritchard et al., 2009; Scheuchl et al., 2016; Wouters et al., 2015). However, there are large glacier-to-glacier variations in recent changes. Even adjacent glacier that have experienced similar rates of ocean and atmospheric warming, have not retreated and thinned uniformly (Larsen et al., 2016; Motyka et al., 2017). In this study, we have shown that the response of glacier thickness to surface mass balance and ocean forcing (section 4.1) becomes weaker for steeper prograde bed slopes. These findings are in agreement with Felikson et al. (2017), who show that almost all thinning observed at marine-terminating glaciers in West Greenland occurs downstream of steep regions of prograde bed slope. Additionally, through analytic expressions for marine-terminating glacier sensitivity to forcing, we show that stronger nonlinearity in forcing processes make glaciers more sensitive to external forcing. As we argue in section 4.2, the timing of forcing onset may also have a significant influence on the current magnitude and rate of glacier response, even for glaciers that are otherwise identical.

The observed retreat and thinning of marine-terminating glaciers in recent decades is striking, but should be interpreted within the context of expected glacier variability forced by stationary stochastic variability in ocean and atmospheric forcing. A few longer records of marine-terminating glacier variability (up to 150 years) have been constructed from airborne and field observations (e.g., Bjørk et al., 2012; Csatho et al., 2008; Lea et al., 2014; Leclercq et al., 2012, 2014; Weidick et al., 2012; Yde & Knudsen, 2007). Though such records are still not long enough to capture the slow time scale of marine-terminating glacier variability ($T_S >$ 1,000 years), detectable changes in atmospheric and ocean warming and the associated terminus retreat only began in the last few decades at most calving glaciers (Bjørk et al., 2012; Leclercq et al., 2014). Even if natural variability of these glaciers is large, it is only expressed on long time scales. Forced change on shorter time scales may exhibit a faster rate of change than what can be reliably attributed to natural variability. We intend to explore such questions of detection and attribution in future work.

The lack of observed thinning and retreat at some glaciers (e.g., Petermann Glacier and ice streams in the western Ross Sea region, see Fountain et al., 2017; Hogg et al., 2016) does not necessarily preclude future thinning and retreat occurring on the slow time scale of hundreds to thousands of years. Indeed, as we have shown (section 4.2), recent changes at these stable marine-terminating glaciers are just a small fraction of the total committed retreat expected in the future in response to climate change that has already occurred. If the trend in climate forcing continues over the next century, there will be many marine-terminating glaciers where the speed of glacier change will accelerate significantly. Even past changes in climate that do not continue into the future cause a *commitment* to future changes in marine-terminating glaciers that persists for hundreds to thousands of years.

6.2. Model Flexibility and Simplicity

The flexibility of the two-stage model has allowed us to analyze the physical processes controlling the response of marine-terminating glaciers to forcing. This flexibility is premised on the assumptions that mass enters the glacier through a spatially averaged surface mass balance and leaves via flux through the grounding line, where that flux is a function of the local ice thickness at flotation. Most of our analysis does not require any further assumptions regarding the physical processes in the grounding zone. Thus, the two-stage model and the associated linear analysis can accommodate a variety of different types of marine-terminating glaciers, including those with strong lateral shear stresses (Hindmarsh, 2012), Weertman basal sliding (Schoof, 2007a), Coulomb plastic failure near the grounding line (V. C. Tsai et al., 2015) or strong buttressing by ice shelves (Haseloff & Sergienko, 2018).

There are some drawbacks to the simplicity of the two-stage model. Our model formulation implicitly assumes that the glacier is marine terminating and always remains marine terminating. Also, as we have shown in section 2.2, the two-stage model emulates the transient behavior of a flowline model at time scales longer than a few decades. However, the flowline model is itself a simplification of real marine-terminating glacier processes, for which there are very few observations. It is difficult to compare the two-stage model directly to observations, since we have shown that the largest changes in stable marine-terminating glaciers occur on time scales that are much longer than the length of available observational time series. We have also shown that the two-stage model may not be entirely reliable for reproducing glacier fluctuations on time scales shorter than a few decades, though the magnitude of glacier response at these short time scales is small (and

it is unclear how well fast glacier fluctuations are simulated in the flowline model). Furthermore, the flux formulation we use (from Haseloff & Sergienko, 2018) integrates the effects of buttressing over the entire ice shelf by assuming that it is at a steady state, and so neglects time-dependent adjustment processes occurring within the ice shelf. A fully coupled model of an ice sheet and ice shelf would likely have an additional time scale associated with ice shelf adjustment processes.

One possible future extension of the two-stage model would be to formulate the linear response problem outlined in section 3 for the spatially extended shelfy-stream equations (what is solved by the flowline model described in section 2.2). One could then find the spatially dependent glacier response to external forcing with a generic spatial structure (rather than the spatially uniform forcing used in the two-stage model), which may include very rapid glacier responses (i.e., shorter than the fast time scale T_F) to spatially localized forcing.

There are also clear limits to the use of a linear theory to capture the complexity of bed topography. In our linearized analysis, we assume that the width-averaged depth and slope of the bed at the grounding line remains relatively unchanged under changes in glacier state. This may be most appropriate for beds with relatively weak topographic variation such as those in West Antarctica, and less appropriate for beds with strong topographic variation, such as those in parts of Greenland. We can, however, still use the two-stage model to calculate the grounding line migration over these bumpy beds. We may also use an *average* depth and bed slope over the region of bed that we expect the grounding line to migrate, which will improve the linear prediction of grounding line migration over bumpy beds on long time scales.

We have also left out other processes, such as isostatic bedrock adjustment, that may be important on the long time scales over which marine-terminating glaciers respond to forcing. Feedbacks between surface mass balance and geometry, such as the height-mass balance feedback, may also play a role. To incorporate such effects (as does Harrison et al., 2003), we might replace the surface mass balance term (P) in equation (8), with a term that depends on H and L. In this study, we consider the limit where the sensitivity of ice fluxes to changes in ice sheet geometry (e.g., $\frac{\partial Q_g}{\partial L}$ and $\frac{\partial Q}{\partial H}$) is much more important to glacier evolution than the sensitivity of surface mass balance to changes in geometry ($\frac{\partial P}{\partial H}$). However, we do not rule out the possibility that when the vertical gradient in surface mass balance gradient is large (due to orographic or other local climate effects), this effect may be important. The virtue of the two-stage model presented here is that the essence of the dynamical system can be identified and explored. These essential dynamics will also operate in more complicated numerical models, in addition to the real glacier system.

7. Conclusions

We have shown that a simple two-stage model can emulate the transient response of a marine-terminating glacier simulated in a spatially extended model, particularly at time scales longer than a few decades. In both the two-stage and spatially extended models, the response of a marine-terminating glacier to forcing is dominated by two time scales. The fast time scale is controlled by the rate of advective adjustment to changes in ice thickness and is typically decades to centuries. The slow time scale is controlled by the rate at which ice thickness perturbations are dissipated by differences in advective and extensional adjustment in the grounding zone and is typically millennia. The slow time scale becomes unstable on shallow prograde slopes and the fast time scale becomes unstable on steep retrograde slopes, producing two distinct forms of the marine ice sheet instability.

We have derived simple expressions for the magnitude of glacier response to different types of forcing that can be calculated without resorting to use of a complex numerical glacier model. The strength of the response depends on the glacier state, the time-averaged forcing, and the strength of nonlinearity in ice dynamical processes. A stable marine-terminating glacier responds slowly to the onset of a trend in forcing and will only begin to approach the long-term expected rate of change on the slow time scale of centuries to millennia. We expect that the current level of stable marine-terminating glacier retreat is a small fraction of the *committed* retreat that can be expected as the rate of glacier change accelerates in coming centuries (as has been shown for many mountain glaciers, e.g., Rupper et al., 2012). Even stable glaciers which have not yet undergone detectable change may undergo such change in the future as the glaciers catch to the forcing. The slow glacier response to stochastic external forcing suggests that the rate, rather than the absolute level, of glacier change caused by trends in forcing are potentially more easily discernible from background noise. Finally, we have shown that the equilibrium state of a marine-terminating glacier depends on the magnitude of noise in nonlinear forcing processes, such as ice shelf length variations that occur through calving.

One important conclusion of this study is that the slow time scale of marine-terminating glacier change ensures that uncertainties in climate forcing (either in the past or future) influence glacier change for hundreds to thousands of years. To account for the uncertainties associated with future climate forcing in simulating ice sheet change will require large ensembles of stochastic ice sheet model simulations that result in probabilistic forecasts of future sea level rise. Though studies such as the SeaRISE project consider uncertainties in ice sheet physics through small multimodel ensembles with common forcing (Bindschadler et al., 2013), they do not capture the uncertainty in future projections associated with the forcing itself (e.g., C. Y. Tsai et al., 2017). As we have shown, considering noise is not just important for constraining the background envelope of variability but also for accurately simulating the time-averaged glacier state. For one, if the magnitude of noise in certain ice sheet processes changes over time (e.g., as the style of iceberg calving from an ice shelf changes), this may drive glacier retreat that would not be predicted in the absence of noise. Also, model spin-up and calibration performed without natural sources of noisy forcing (or forcing with a truncated spectrum of variability due to asynchronous model coupling) may lead to unrealistic glacier states. As a new generation of fully coupled climate and ice sheet models are used to produce projections of future ice sheet change, it is important to consider the ice sheet response to high-frequency climate variability through nearly synchronous coupling. To exclude the noise of climate when predicting future ice sheet change misses an important piece of the glaciological puzzle.

Acknowledgments

Source code and documentation of the two-stage and flowline models used in this study are freely available as public repositories on GitHub: https://github.com/aarobel/. Thanks to Olga Sergienko, Martin Truffer, Jeremy Bassis, and Elisa Mantelli for helpful comments on the manuscript. This work was initially conceived through a series of conversations at the 2014 Advanced Climate Dynamics Course, which is coordinated by the Norwegian Research School in Climate Dynamics (ResClim). Thanks to Nicholas Beaird, Bradley Markle, and Andreas Vieli for taking part in those initial conversations. The authors also thank Christian Schoof, Victor Tsai, Georgy Manucharyan, John Christian, Denis Felikson, and Ian Joughin for subsequent conversations and suggestions. A. A. R. was supported by the NOAA Climate and Global Change Postdoctoral Fellowship during part of this project. G. H. R. acknowledges support from NSF PLR-1643299. M. H. was supported by the Princeton AOS Postdoctoral and Visiting Scientist Program.

References

Amundson, J. M. (2016). A mass-flux perspective of the tidewater glacier cycle. *Journal of Glaciology*, *62*(231), 82–93.

Bassis, J. N. (2011). The statistical physics of iceberg calving and the emergence of universal calving laws. *Journal of Glaciology*, *57*(201), 3–16.

Bindschadler, R. A., Nowicki, S., Abe-Ouchi, A., Aschwanden, A., Choi, H., Fastook, J., et al. (2013). Ice-sheet model sensitivities to environmental forcing and their use in projecting future sea level (the SeaRISE project). *Journal of Glaciology*, *59*(214), 195–224.

Bjørk, A. A., Kjær, K. H., Korsgaard, N. J., Khan, S. A., Kjeldsen, K. K., Andresen, C. S., et al. (2012). An aerial view of 80 years of climate-related glacier fluctuations in southeast Greenland. *Nature Geoscience*, *5*(6), 427–432.

Box, G., Jenkins, G., Reinsel, G., & Ljung, G. (2015). *Time series analysis: Forecasting and control*. Hobokin, New Jersey: Wiley Series in Probability and Statistics, Wiley.

Brinkerhoff, D., Truffer, M., & Aschwanden, A. (2017). Sediment transport drives tidewater glacier periodicity. *Nature Communications*, *8*(1), 90.

Brondex, J., Gagliardini, O., Gillet-Chaulet, F., & Durand, G. (2017). Sensitivity of grounding line dynamics to the choice of the friction law. *Journal of Glaciology*, *63*(241), 854–866.

Csatho, B., Schenk, T., Van Der Veen, C. J., & Krabill, W. B. (2008). Intermittent thinning of Jakobshavn Isbrae, West Greenland, since the Little Ice Age. *Journal of Glaciology*, *54*(184), 131–144.

Csatho, B. M., Schenk, A. F., van der Veen, C. J., Babonis, G., Duncan, K., Rezvanbehbahani, S., et al. (2014). Laser altimetry reveals complex pattern of Greenland ice sheet dynamics. *Proceedings of the National Academy of Sciences*, *111*(52), 18,478–18,483.

Cuffey, K., & Paterson, W. (2010). *The physics of Glaciers* (3rd ed.). Amsterdam, Boston: Pergamon.

Drouet, A.-S., Docquier, D., Durand, G., Hindmarsh, R., Pattyn, F., Gagliardini, O., & Zwinger, T. (2013). Grounding line transient response in marine ice sheet models. *The Cryosphere*, *7*(2), 395–406.

Favier, L., Durand, G., Cornford, S., Gudmundsson, G., Gagliardini, O., Gillet-Chaulet, F., et al. (2014). Retreat of Pine Island glacier controlled by marine ice-sheet instability. *Nature Climate Change*, *4*, 117–121.

Felikson, D., Bartholomaus, T. C., Catania, G. A., Korsgaard, N. J., Kjær, K. H., Morlighem, M., et al. (2017). Inland thinning on the Greenland ice sheet controlled by outlet glacier geometry. *Nature Geoscience*, *10*, 366–369.

Fettweis, X. (2007). Reconstruction of the 1979–2006 Greenland ice sheet surface mass balance using the regional climate model MAR. *The Cryosphere*, *1*(1), 21–40.

Fountain, A. D., Glenn, B., & Scambos, T. A. (2017). The changing extent of the glaciers along the western Ross Sea, Antarctica. *Geology*, *45*, 927–930. https//doi.org/10.1130/G39240.1

Fyke, J. G., Vizcaíno, M., & Lipscomb, W. H. (2014). The pattern of anthropogenic signal emergence in Greenland ice Sheet surface mass balance. *Geophysical Research Letters*, *41*, 6002–6008. https//doi.org/10.1002/2014GL060735

Gomez, N., Mitrovica, J. X., Huybers, P., & Clark, P. U. (2010). Sea level as a stabilizing factor for marine-ice-sheet grounding lines. *Nature Geoscience*, *3*(12), 850–853.

Gudmundsson, G., Krug, J., Durand, G., Favier, L., & Gagliardini, O. (2012). The stability of grounding lines on retrograde slopes. *The Cryosphere*, *6*(4), 2597–2619.

Harrison, W. D., Raymond, C. F., Echelmeyer, K. A., & Krimmel, R. M. (2003). A macroscopic approach to glacier dynamics. *Journal of Glaciology*, *49*(164), 13–21.

Haseloff, M., & Sergienko, O. V. (2018). The effect of buttressing on grounding line dynamics. *Journal of Glaciology*, *64*(245), 417–431. https//doi.org/10.1017/jog.2018.30

Hindmarsh, R. C. (2012). An observationally validated theory of viscous flow dynamics at the ice-shelf calving front. *Journal of Glaciology*, *58*(208), 375–387.

Hindmarsh, R., & Le Meur, E. (2001). Dynamical processes involved in the retreat of marine ice sheets. *Journal of Glaciology*, *47*(157), 271–282.

Hogg, A. E., Shepherd, A., Gourmelen, N., & Engdahl, M. (2016). Grounding line migration from 1992 to 2011 on Petermann glacier, North-West Greenland. *Journal of Glaciology*, *62*(236), 1104–1114.

Intergovernmental Panel on Climate Change, IPCC (2013). *Climate Change 2013: The Physical Science Basis. Contribution of Working Group I to the Fifth Assessment Report of the Intergovernmental Panel on Climate Change* (p. 1535). Cambridge, United Kingdom and New York, NY, USA: Cambridge University Press. https//doi.org/10.1017/CBO9781107415324

Jamieson, S., Vieli, A., Livingstone, S., Cofaigh, C., Stokes, C., Hillenbrand, C., & Dowdeswell, J. (2012). Ice-stream stability on a reverse bed slope. *Nature Geoscience*, *5*(11), 799–802.
Jóhannesson, T., Raymond, C., & Waddington, E. (1989). Time-scale for adjustment of glaciers to changes in mass balance. *Journal of Glaciology*, *35*(121), 355–369.
Joughin, I., Alley, R. B., & Holland, D. M. (2012). Ice-sheet response to oceanic forcing. *Science*, *338*(6111), 1172–1176.
Joughin, I., Howat, I. M., Fahnestock, M., Smith, B., Krabill, W., Alley, R. B., et al. (2008). Continued evolution of Jakobshavn Isbræ following its rapid speedup. *Journal of Geophysical Research*, *113*, F04006. https//doi.org/10.1029/2008JF001023
Joughin, I., Smith, B. E., Howat, I. M., Scambos, T., & Moon, T. (2010). Greenland flow variability from ice-sheet-wide velocity mapping. *Journal of Glaciology*, *56*(197), 415–430.
Larsen, S. H., Khan, S. A., Ahlstrøm, A. P., Hvidberg, C. S., Willis, M. J., & Andersen, S. B. (2016). Increased mass loss and asynchronous behavior of marine-terminating outlet glaciers at Upernavik Isstrøm, NW Greenland. *Journal of Geophysical Research: Earth Surface*, *121*, 241–256. https//doi.org/10.1002/2015JF003507
Lea, J., Mair, D., Nick, F., Rea, B., Van As, D., Morlighem, M., et al. (2014). Fluctuations of a Greenlandic tidewater glacier driven by changes in atmospheric forcing: Observations and modelling of Kangiata Nunaata Sermia, 1859–present. *The Cryosphere Discussions*, *8*, 2031–2045.
Leclercq, P. W., Oerlemans, J., Basagic, H. J., Bushueva, I., Cook, A., & Le Bris, R. (2014). A data set of worldwide glacier length fluctuations. *The Cryosphere*, *8*(2), 659–672.
Leclercq, P., Weidick, A., Paul, F., Bolch, T., Citterio, M., & Oerlemans, J. (2012). Brief communication: Historical glacier length changes in West Greenland. *The Cryosphere*, *6*, 1339–1343.
Lenton, T. M. (2011). Early warning of climate tipping points. *Nature Climate Change*, *1*(4), 201–209.
Lingle, C. S. (1984). A numerical model of interactions between a polar ice stream and the ocean: Application to ice stream E, West Antarctica. *Journal of Geophysical Research*, *89*(C3), 3523–3549.
Lüthi, M. P. (2009). Transient response of idealized glaciers to climate variations. *Journal of Glaciology*, *55*(193), 918–930.
Mantelli, E., Bertagni, M. B., & Ridolfi, L. (2016). Stochastic ice stream dynamics. *Proceedings of the National Academy of Sciences*, *113*(32), E4594—E4600.
Marzeion, B., Cogley, J. G., Richter, K., & Parkes, D. (2014). Attribution of global glacier mass loss to anthropogenic and natural causes. *Science*, *345*(6199), 919–921.
Mernild, S. H., Mote, T. L., & Liston, G. E. (2011). Greenland ice sheet surface melt extent and trends: 1960–2010. *Journal of Glaciology*, *57*(204), 621–628.
Mikkelsen, T. B., Grinsted, A., & Ditlevsen, P. (2017). Influence of temperature fluctuations on equilibrium ice sheet volume. *The Cryosphere Discussions*, *2017*, 1–16. https//doi.org/10.5194/tc-2017-47
Moon, T., Joughin, I., & Smith, B. (2015). Seasonal to multiyear variability of glacier surface velocity, terminus position, and sea ice/ice mélange in northwest Greenland. *Journal of Geophysical Research: Earth Surface*, *120*, 818–833. https//doi.org/10.1002/2015JF003494
Motyka, R. J., Cassotto, R., Truffer, M., Kjeldsen, K. K., Van As, D., Korsgaard, N. J., et al. (2017). Asynchronous behavior of outlet glaciers feeding Godthåbsfjord (Nuup Kangerlua) and the triggering of Narsap Sermia's retreat in SW Greenland. *Journal of Glaciology*, *63*(238), 288–308.
Mulder, T. E., Baars, S., Wubs, F. W., & Dijkstra, H. A. (2018). Stochastic marine ice sheet variability. *Journal of Fluid Mechanics*, *843*, 748–777. https//doi.org/10.1017/jfm.2018.148
Nick, F., Van der Veen, C. J., Vieli, A., & Benn, D. (2010). A physically based calving model applied to marine outlet glaciers and implications for the glacier dynamics. *Journal of Glaciology*, *56*(199), 781–794.
Nicolis, C., & Nicolis, G. (1981). Stochastic aspects of climatic transitions–additive fluctuations. *Tellus*, *33*(3), 225–234.
Nye, J. (1960). The response of glaciers and ice-sheets to seasonal and climatic changes. *Proceedings of the Royal Society of London A: Mathematical, Physical and Engineering Sciences*, *256*(1287), 559–584.
Nye, J. (1963a). On the theory of the advance and retreat of glaciers. *Geophysical Journal International*, *7*(4), 431–456.
Nye, J. (1963b). The response of a glacier to changes in the rate of nourishment and wastage. *Proceedings of the Royal Society of London A: Mathematical, Physical and Engineering Sciences*, *275*(1360), 87–112.
Nye, J. F. (1965). The frequency response of glaciers. *Journal of Glaciology*, *5*(41), 567–587.
Oerlemans, J. (2000). Holocene glacier fluctuations: Is the current rate of retreat exceptional?*Annals of Glaciology*, *31*(1), 39–44.
Park, J., Gourmelen, N., Shepherd, A., Kim, S., Vaughan, D., & Wingham, D. (2013). Sustained retreat of the Pine Island glacier. *Geophysical Research Letters*, *40*, 2137–2142. https//doi.org/10.1002/grl.50379
Pattyn, F., Schoof, C., Perichon, L., Hindmarsh, R., Bueler, E., Fleurian, B. d., et al. (2012). Results of the marine ice sheet model intercomparison project, MISMIP. *The Cryosphere*, *6*(3), 573–588.
Pegler, S. S. (2016). The dynamics of confined extensional flows. *Journal of Fluid Mechanics*, *804*, 24–57.
Pelto, M. S., & Warren, C. R. (1991). Relationship between tidewater glacier calving velocity and water depth at the calving front. *Annals of Glaciology*, *15*, 115–118.
Penland, C. (2003). A stochastic approach to nonlinear dynamics: A review. *Bulletin of the American Meteorological Society*, *84*(7), 925–925.
Post, A., & Motyka, R. J. (1995). Taku and Le Conte glaciers, Alaska: Calving-speed control of late-holocene asynchronous advances and retreats. *Physical Geography*, *16*(1), 59–82.
Pritchard, H. D., Arthern, R. J., Vaughan, D. G., & Edwards, L. A. (2009). Extensive dynamic thinning on the margins of the Greenland and Antarctic ice sheets. *Nature*, *461*(7266), 971–975.
Rignot, E., Koppes, M., & Velicogna, I. (2010). Rapid submarine melting of the calving faces of West Greenland glaciers. *Nature Geoscience*, *3*(3), 187–191.
Robel, A., Schoof, C., & Tziperman, E. (2014). Rapid grounding line migration induced by internal ice stream variability. *Journal of Geophysical Research: Earth Surface*, *119*, 2430–2447. https//doi.org/10.1002/2014JF003251
Roe, G. H., & Baker, M. B. (2014). Glacier response to climate perturbations: An accurate linear geometric model. *Journal of Glaciology*, *60*(222), 670–684.
Roe, G. H., & Baker, M. B. (2016). The response of glaciers to climatic persistence. *Journal of Glaciology*, *62*(233), 440–450.
Roe, G. H., Baker, M. B., & Herla, F. (2017). Centennial glacier retreat as categorical evidence of regional climate change. *Nature Geoscience*, *10*(2), 95–99.
Roe, G. H., & O'Neal, M. A. (2009). The response of glaciers to intrinsic climate variability: Observations and models of late-Holocene variations in the Pacific Northwest. *Journal of Glaciology*, *55*(193), 839–854.
Rupper, S., Schaefer, J. M., Burgener, L. K., Koenig, L. S., Tsering, K., & Cook, E. R. (2012). Sensitivity and response of Bhutanese glaciers to atmospheric warming. *Geophysical Research Letters*, *39*, L19503. https//doi.org/10.1029/2012GL053010

Scheuchl, B., Mouginot, J., Rignot, E., Morlighem, M., & Khazendar, A. (2016). Grounding line retreat of Pope, Smith, and Kohler glaciers, West Antarctica, measured with Sentinel-1a radar interferometry data. *Geophysical Research Letters*, *43*, 8572–8579. https//doi.org/10.1002/2016GL069287

Schodlok, M. P., Menemenlis, D., Rignot, E., & Studinger, M. (2012). Sensitivity of the ice-shelf/ocean system to the sub-ice-shelf cavity shape measured by NASA IceBridge in Pine Island glacier, West Antarctica. *Annals of Glaciology*, *53*(60), 156–162.

Schoof, C. (2006). A variational approach to ice stream flow. *Journal of Fluid Mechanics*, *556*, 227–251. https//doi.org/10.1017/S0022112006009591

Schoof, C. (2007a). Marine ice-sheet dynamics. Part 1. The case of rapid sliding. *Journal of Fluid Mechanics*, *573*, 27–55. https//doi.org/10.1017/S0022112006003570

Schoof, C. (2007b). Ice sheet grounding line dynamics: Steady states, stability, and hysteresis. *Journal of Geophysical Research*, *112*, F03S28. https//doi.org/10.1029/2006JF000664

Schoof, C. (2012). Marine ice sheet stability. *Journal of Fluid Mechanics*, *698*, 62–72.

Schoof, C., Davis, A. D., & Popa, T. V. (2017). Boundary layer models for calving marine outlet glaciers. *The Cryosphere Discussions*, *11*, 1–30. https//doi.org/10.5194/tc-2017-42

Sciascia, R., Straneo, F., Cenedese, C., & Heimbach, P. (2013). Seasonal variability of submarine melt rate and circulation in an East Greenland fjord. *Journal of Geophysical Research: Oceans*, *118*, 2492–2506. https//doi.org/10.1002/jgrc.20142

Seroussi, H., Nakayama, Y., Larour, E., Menemenlis, D., Morlighem, M., Rignot, E., & Khazendar, A. (2017). Continued retreat of Thwaites glacier, West Antarctica, controlled by bed topography and ocean circulation. *Geophysical Research Letters*, *44*, 6191–6199. https//doi.org/10.1002/2017GL072910

Suzuki, M. (1977). Scaling theory of transient phenomena near the instability point. *Journal of Statistical Physics*, *16*(1), 11–32.

Tsai, C.-Y., Forest, C. E., & Pollard, D. (2017). Assessing the contribution of internal climate variability to anthropogenic changes in ice sheet volume. *Geophysical Research Letters*, *44*, 6261–6268. https//doi.org/10.1002/2017GL073443

Tsai, V. C., Stewart, A. L., & Thompson, A. F. (2015). Marine ice-sheet profiles and stability under Coulomb basal conditions. *Journal of Glaciology*, *61*(226), 205–215.

van der Veen, C. (2001). Greenland ice sheet response to external forcing. *Journal of Geophysical Research*, *106*(D24), 34,047–34,058.

Velicogna, I. (2009). Increasing rates of ice mass loss from the Greenland and Antarctic ice sheets revealed by GRACE. *Geophysical Research Letters*, *36*, L19503. https//doi.org/10.1029/2009GL040222

Weertman, J. (1957). On the sliding of glaciers. *Journal of Glaciology*, *3*(21), 33–38.

Weertman, J. (1974). Stability of the junction of an ice sheet and an ice shelf. *Journal of Glaciology*, *13*, 3–11.

Weidick, A., Bennike, O., Citterio, M., & Nørgaard-Pedersen, N. (2012). Neoglacial and historical glacier changes around Kangersuneq fjord in southern West Greenland. *Geological Survey of Denmark and Greenland Bulletin*, *27*, 68.

Wouters, B., Martin-Español, A., Helm, V., Flament, T., van Wessem, J., Ligtenberg, S., et al. (2015). Dynamic thinning of glaciers on the Southern Antarctic Peninsula. *Science*, *348*(6237), 899–903.

Yde, J. C., & Knudsen, N. T. (2007). 20th-century glacier fluctuations on Disko Island (Qeqertarsuaq), Greenland. *Annals of Glaciology*, *46*(1), 209–214.